Title
Poor Outlook for 4d and 5d Kitaev Candidate Materials: Density Functional Theory Calculations Point to Small Kitaev Terms

Author
Eth, Daniel Ross

Publication Date
2020

Peer reviewed|Thesis/dissertation

UNIVERSITY OF CALIFORNIA

Los Angeles

Poor Outlook for 4*d* and 5*d* Kitaev Candidate Materials:

Density Functional Theory Calculations Point to Small Kitaev Terms

A dissertation submitted in partial satisfaction

of the requirements for the degree

Doctor of Philosophy in Materials Science and Engineering

by

Daniel Ross Eth

2020

ABSTRACT OF THE DISSERTATION

Poor Outlook for 4*d* and 5*d* Kitaev Candidate Materials:

Density Functional Theory Calculations Point to Small Kitaev Terms

by

Daniel Ross Eth

Doctor of Philosophy in Materials Science and Engineering

University of California, Los Angeles, 2020

Professor Dwight Christopher Streit, Chair

Na_2IrO_3 and other "Kitaev candidate" materials are of much scientific and technological interest. In such materials, proposed anisotropic, Ising-like interactions promote magnetic frustration, potentially leading to a quantum spin liquid (QSL) ground state with excitations (non-Abelian anyons) that could enable *topological quantum computing* – a form of quantum computing particularly robust to decoherence. Unfortunately, experimental work indicates that Na_2IrO_3 and other Kitaev candidates do not exhibit a QSL ground state. While there are several proposals for manipulating Kitaev candidates into a QSL state, there is no consensus over whether the effective-spin interactions of these materials are proximate to the values necessary for such a state. Here, we use density functional theory (DFT) and mathematical techniques to investigate the electronic properties and effective-spin interactions of Kitaev candidate materials. Our approach for

determining spin interaction terms, Compressive Sensing Spin Dynamics (CSSD), involves two main steps: 1) by appending the Kohn-Sham energy functional with a Lagrangian term that allows for quickly finding the lowest energy solution of a material given fixed magnetic moments, we perform many calculations of the material with the spins slightly perturbed from the equilibrium state; 2) we perform compressive sensing on these data (on the fixed spins and magnetic fields required to stabilize the desired spin arrangement) to yield the interaction terms with far fewer data than otherwise required. Performing this procedure on the Kitaev candidates Na_2IrO_3 and α-$RuCl_3$ indicates neither is close to the Kitaev QSL regime. We further investigate manipulated versions of Kitaev candidate materials and find all have problems: epitaxial and single layers of Na_2IrO_3 are conductors (implying Na_2IrO_3 cannot be cleanly separated into individual layers without changing the band structure), while straining Na_2IrO_3 in-plane introduces different problems if under tension (the Ir-O-Ir angles increase, leading to less destructive interference of undesirable interactions) and compression (the Ir-Ir distances decrease, leading to larger isotropic Heisenberg interaction, which competes with the Kitaev interaction). We additionally use CSSD to evaluate the interaction terms of idealized versions of Na_2IrO_3 and α-$RuCl_3$ (90° Ir-O-Ir and Ru-Cl-Ru angles), and our results indicate that these, too, are far from the Kitaev QSL state. Finally, we investigate if $YbBr_3$, as a lanthanide material, may circumvent the problems with 4*d* and 5*d* candidates, due to smaller *f*-*f* orbital overlap compared to *d*-*d* overlap. While the results with $YbBr_3$ are somewhat ambiguous, we conclude *f*-orbital Kitaev candidate materials warrant further investigation.

The dissertation of Daniel Ross Eth is approved.

Bruce S. Dunn

Jaime Marian

Vidvuds Ozoliņš

Dwight Christopher Streit, Committee Chair

University of California, Los Angeles

2020

TABLE OF CONTENTS

LIST OF FIGURES

LIST OF TABLES

VITA

2014 – 2020	Graduate Student Researcher Department of Materials Science and Engineering, UCLA
2017 – 2019	Visiting Assistant in Research Department of Applied Physics, Yale University
Autumn 2017	Teaching Fellow Department of Applied Physics, Yale University
2014	M.S. in Materials Science and Engineering, Stanford University
2014	B.S. in Materials Science and Engineering, Stanford University

Introduction

Recently, there has been much interest in Na_2IrO_3 and other "Kitaev candidate" materials. In such materials, it is hypothesized that anisotropic, Ising-like "Kitaev" interactions promote magnetic frustration, potentially leading to a quantum spin liquid (QSL) ground state.[1] Due to the layered, two-dimensional structure of these materials, realization of a Kitaev QSL could allow for quasiparticles known as *anyons* – in particular, yet to be observed *non-Abelian anyons*.

Anyons are peculiar in that the statistics they follow are neither Fermi-Dirac nor Bose-Einstein. For fermions and bosons, adiabatically exchanging two indistinguishable particles is represented by multiplying the two-particle wave function by -1 or +1, respectively.

$$|\psi_1\psi_2\rangle = \pm|\psi_2\psi_1\rangle.$$

In three dimensions, these are the only two options, and all elementary particles are either fermions or bosons. This is because exchanging two particles twice is topologically equivalent to one particle circling around another, which is topologically equivalent to doing nothing, and thus must result in the original wave function (Figure 1).

Figure 1: In 3D, circling one particle around another is topologically equivalent to doing nothing.

For two-dimensional quasiparticles, however, the situation can be different. One quasiparticle circling another is no longer topologically equivalent to doing nothing, since it is impossible to deform the path of the circling quasiparticle to a point without the path hitting the other quasiparticle (Figure 2).

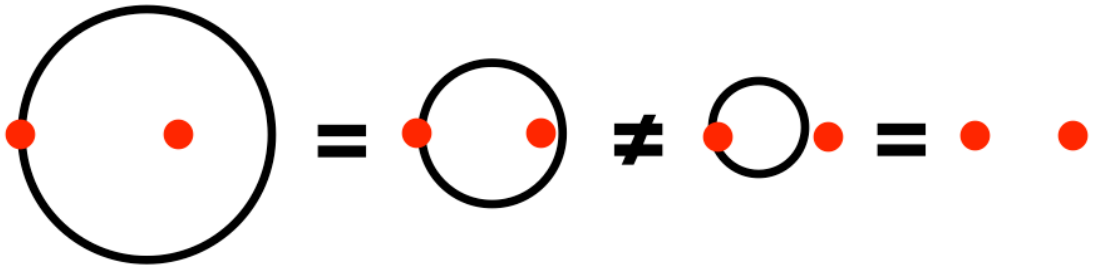

Figure 2: In 2D, circling one particle around another is not topologically equivalent to doing nothing.

In two-dimensions, adiabatically exchanging two quasiparticles twice does not need to result in the original wave function, but instead can introduce an arbitrary phase. Exchanging the two quasiparticles can thus be expressed as:

$$|\psi_1\psi_2\rangle = e^{i\theta}|\psi_2\psi_1\rangle \qquad (\theta \text{ is a real number}),$$

where the exchange takes place through the particles rotating counterclockwise (a clockwise rotation would instead multiply the wave function by $e^{-i\theta}$). Since introducing separate phases to the wave function is commutative, "braiding" several of such quasiparticles is also commutative. Quasiparticles that follow such statistics are known as *Abelian anyons*.[2]

On the other hand, if the system contains degeneracy, with m distinct states associated with the same quasiparticle configuration, then adiabatically exchanging quasiparticles can not only add a phase to the wave function, but also can send the system

into a different state associated with the same configuration. Adiabatically exchanging quasiparticles then can be represented by an m x m unitary matrix acting on the states. Since matrix multiplication need not commute, braiding the quasiparticles need not, either. Quasiparticles that follow such non-commutative braiding statistics are known as *non-Abelian anyons*.

$$\psi_a = R\psi_b \qquad (R \text{ is an } m \text{ x } m \text{ unitary matrix}).$$

Non-Abelian anyons hold much technological potential, as they might allow for a particularly robust and scalable form of quantum computing known as *topological quantum computing*.

Unfortunately, attempts to create non-Abelian anyons in spin systems have so far failed or yielded inconclusive results. Na_2IrO_3, while initially hypothesized to yield a QSL ground state (allowing for non-Abelian anyons), instead gives an antiferromagnetic "zigzag" order.[3, 4] It has been proposed that Na_2IrO_3 may be able to be coaxed into a QSL via manipulation, such as through doping or growing layers on a substrate.[5] α-$RuCl_3$, another Kitaev candidate material, has shown evidence of being coaxed into a QSL under application of a magnetic field, but it is not clear whether this QSL is due to Kitaev physics or some other phenomena.[6] It is unclear whether the effective-spin interactions in these materials fall into the parameter regime of the Kitaev-model QSL. Here, we use density-functional theory (DFT) and mathematical techniques to examine the electronic structures and effective-spin interactions of Kitaev candidate materials.

Motivation for Topological Quantum Computing

Robust, large-scale quantum computers could be transformative. While classical computers store information as bits, quantum computers store information as *qubits*. A single qubit can be represented as a superposition of two states ("0" and "1"), and a system of n qubits can be represented as a superposition of 2^n states. An n-qubit system can therefore be represented by a 2^n-dimensional vector, $(a_0, a_1, \ldots, a_{2^n-1})$, where each a_j is a complex number, and where the sum over all j (with j varying from 0 to $2^n - 1$) of $|a_j|^2$ is 1. Quantum logic gates can be described by unitary matrices, where a quantum gate acting on n qubits is represented by a 2^n x 2^n unitary matrix acting on the 2^n-dimensinoal vector that represents the qubits. Typically, at the end of a quantum algorithm, a measurement occurs, collapsing the n qubits into a sequence of n bits, with a measurement corresponding to the j^{th} possible sequence of bits occurring with probability $|a_j|^2$.

Quantum computing offers the potential to solve certain types of problems vastly faster than can classical computers. Prime factorization is one example of such a problem. While the most efficient known classical algorithm for factoring an integer into its constituent primes cannot be achieved in polynomial time, Shor's algorithm – a quantum algorithm – can do just that.[7]

Quantum computers also would be very useful tools for scientific and technological advancement. This appears to be the case especially for certain simulations involving quantum mechanical processes, such as in computational materials science and computational chemistry. With classical computing, the computational cost of quantum mechanical simulations often increases exponentially with system size – making large

simulations intractable. Quantum computers, by contrast, could carry out many such calculations in polynomial time.[8]

Unfortunately, quantum computers have proven quite difficult to build. Google has recently claimed to have achieved *quantum supremacy* – performing a calculation in 200 seconds that would take a state-of-the-art supercomputer approximately 10,000 years.[9] But this demonstration was purely a proof of concept, and a more practical quantum computer capable of performing calculations that we want to perform (beyond simply for the purposes of demonstration) is likely a ways away. The biggest problem is that quantum decoherence can destroy the superposition necessary for quantum computing. Quantum computers are typically isolated and run at low temperatures, but despite this, decoherence generally occurs in seconds or less. While methods for quantum error correction have been proposed, they require an incredibly small error rate and would greatly increase the number of qubits required.

Topological quantum computing could allow for circumventing the problem of quantum decoherence. In topological quantum computing, the qubits are stored in the phases of the wave functions of non-Abelian anyons. Logical operations are carried out by braiding these anyons in specific ways. Decoherence is much less likely in topological quantum computing than in other forms of quantum computing, since the information is stored not locally, but globally, and topological properties aren't affected by local perturbations.

The Kitaev Model

Alexei Kitaev has proposed a model that would allow for non-Abelian anyons, and thus topological quantum computing.[2] This model (the *Kitaev model*) consists of a 2D honeycomb lattice, with spins of 1/2 on each lattice point, and each lattice point linked to its three nearest neighbors. Each link therefore points in one of three directions (with 120° between links), and the links can be labeled as x, y, and z, depending on their direction (Figure 3).

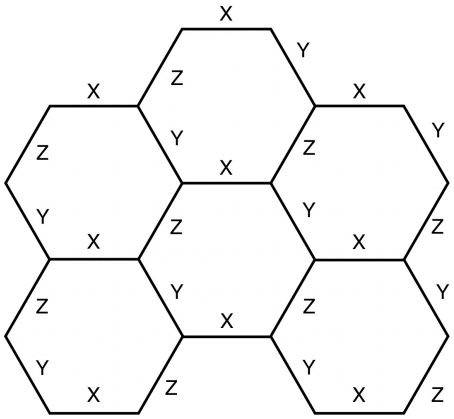

Figure 3: A honeycomb lattice with x, y, and z links, as in the Kitaev model.

Nearest-neighbor spins interact with each other in an anisotropic manner, dependent on the direction of the link between the lattice points. Spins connected by an x-link interact only via their x-component of the spin operator, and so on. This leads to the following Hamiltonian:

$$H = -K_x \sum_{x-links} \sigma_j^x \sigma_k^x - K_y \sum_{y-links} \sigma_j^y \sigma_k^y - K_z \sum_{z-links} \sigma_j^z \sigma_k^z,$$

where K_x, K_y, and K_z are the magnitudes of the interactions along the three links.[2] Kitaev showed how this model is exactly solvable by describing the spin operators in terms of

Majorana fermions. Since the interactions along every link cannot be satisfied simultaneously, there is large magnetic frustration, and the resultant ground state is a QSL. If any of the *K*'s have larger magnitude than the sum of the other two, then there is a gap for all excitations of the ground state, and this phase allows for Abelian anyons. If none of the *K*'s have larger magnitudes than the sum of the other two, then this phase allows for non-Abelian anyons, yet the gap disappears. Applying a magnetic field, however, opens up a gap while still allowing for non-Abelian anyons.

Several candidate materials have been proposed to potentially satisfy the Kitaev model.

Na_2IrO_3

Na_2IrO_3 possesses many characteristics that give it promise as a candidate for the Kitaev model. The basic structure of Na_2IrO_3 is of alternating layers of Na and $NaIr_2O_6$ (Figure 4: left). Within the $NaIr_2O_6$ layers, edge-sharing IrO_6 octahedra form hexagons, creating a honeycomb structure with Na in the center of each hexagon (Figure 4: right). The $NaIr_2O_6$ layers fulfill the 2D honeycomb lattice requirement of the Kitaev model.

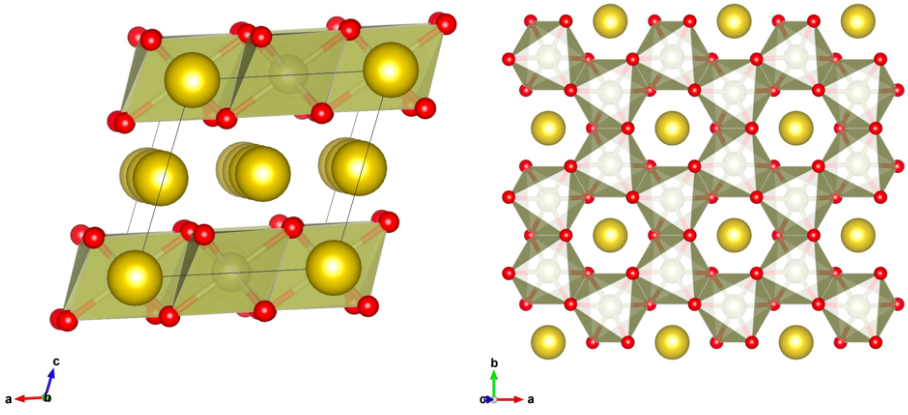

Figure 4: Left- Na_2IrO_3 consists of alternating layers of Na and $NaIr_2O_6$. Right- In the $NaIr_2O_6$ layers, edge sharing IrO_6 octahedra form hexagons. (Figure generated with VESTA.[10])

In IrO_6 octahedra, the crystal field splits the 5*d* orbitals into two higher energy e_g states and three lower energy t_{2g} states (*xy*, *xz*, and *yz*, with Cartesian coordinates corresponding to Ir-O octahedra bond directions). The t_{2g} orbitals in the d^5 configuration of Ir^{4+} contain a hole that has effective angular momentum $l_{eff} = 1$, with $\left|l^z_{eff} = 0\right\rangle \equiv |xy\rangle$ and $\left|l^z_{eff} = \pm 1\right\rangle \equiv -\frac{1}{\sqrt{2}}(i|xz\rangle \pm |yz\rangle)$. The strong spin-orbit coupling (SOC) for Ir splits the three t_{2g} orbitals into a lower-energy, fully filled, effective total angular momentum $j_{eff} = 3/2$ quartet and a higher-energy, half-filled $j_{eff} = 1/2$ Kramers doublet (Figure 5). The SOC also links the moments with reference to the crystal axes via the Kramers doublet states ($|+1/2\rangle = \sin\alpha\,|0,\uparrow\rangle - \cos\alpha\,|+1,\downarrow\rangle$, $|-1/2\rangle = \sin\alpha\,|0,\downarrow\rangle - \cos\alpha\,|-1,\uparrow\rangle$, with α determined by the relative strengths of the SOC and possible tetragonal splitting).[11, 12]

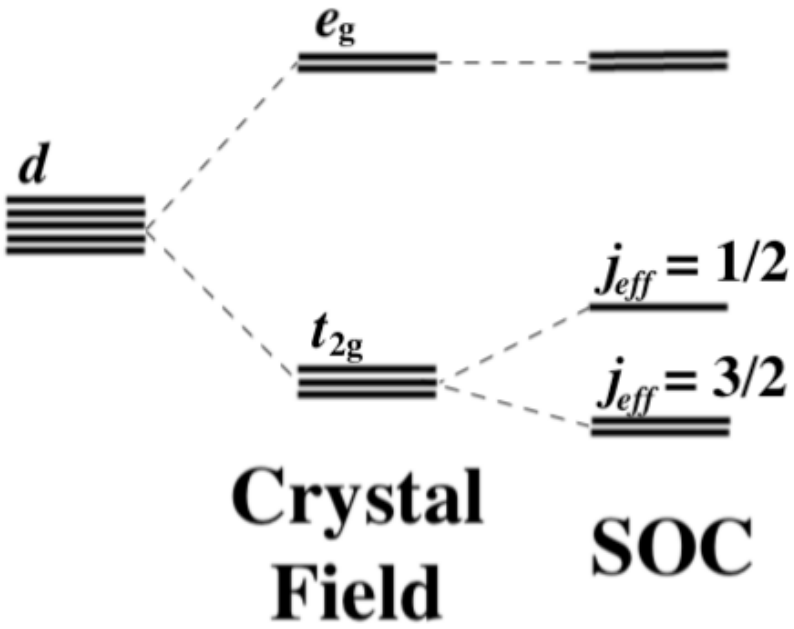

Figure 5: Proposed band structure for Na_2IrO_3, considering the crystal-field splitting and SOC.

Electrons can potentially hop between j_{eff} = 1/2 states on adjacent Ir ions via *p* orbitals on the mutually bonded O ions. Assuming Ir-O-Ir angles of 90°, destructive interference between the two Ir-O-Ir pathways destroys the isotropic part of the interaction, yielding an anisotropic interaction that is bond dependent, implying an effective Kitaev-like Hamiltonian.[12] Competing with this Kitaev interaction, however, is direct Ir-Ir hopping, which results in isotropic, Heisenberg interactions between Ir spins.

Combining these two interactions leads to the *Kitaev-Heisenberg model* (K-H model):[1]

$$H = K\left(\sum_{x-bonds} \sigma_j^x \sigma_k^x + \sum_{y-bonds} \sigma_j^y \sigma_k^y + \sum_{z-bonds} \sigma_j^z \sigma_k^z\right) + J \sum_{all\ bonds} \sigma_j \bullet \sigma_k,$$

where *K* corresponds to the strength of the anisotropic Kitaev interactions, *J* corresponds to the strength of the isotropic Heisenberg interaction, and the summations run over nearest-neighbor Ir-Ir pairs. The definition of x-, y-, and z-bonds are in terms of a Cartesian coordinate system in which the axes are pointed approximately along the Ir-O bonds (that is, from the Ir towards the vertices of the octahedra – though not exactly along these Ir-O bonds as the octahedra are not ideal). In this coordinate system, an Ir-Ir bond is considered an "x-bond" if the two Ir-O-Ir pathways between the specific Ir's are within the yz-plane, and correspondingly for "y-bonds" (Ir-O-Ir pathways in xz-plane) and "z-bonds" (xy-plane) (Figure 6). The component of the spin considered in the Kitaev interaction for each Ir-Ir bond is therefore the component orthogonal to the Ir-O-Ir pathways between the two Ir.

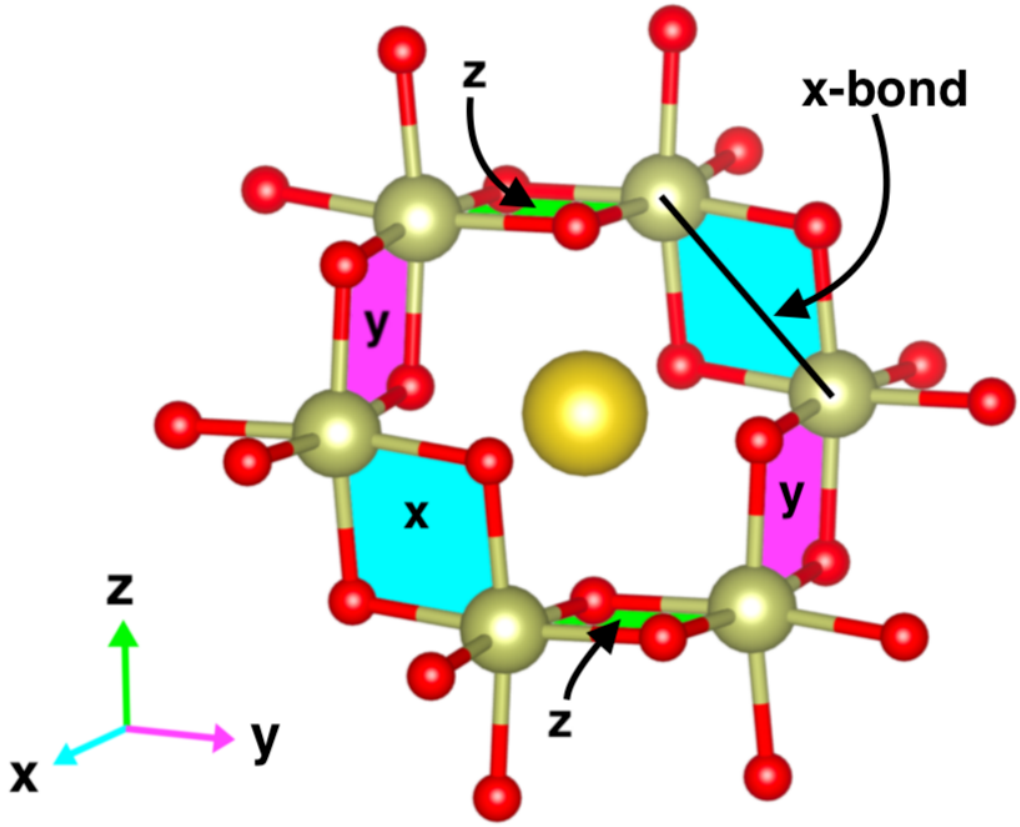

Figure 6: Na_2IrO_3, oriented relative to the Cartesian coordinates used in the K-H model. Bonds between neighboring Ir (olive colored) are labeled with the axis perpendicular to the plane traced by the corresponding Ir-O-Ir pathways. The Ir-Ir x-bonds cut through the yz-plane (blue), and similarly for the y-bonds (magenta) and z-bonds (green). For each Ir-Ir bond, the portion of the spin relevant for the Kitaev interaction is the part along the corresponding axis (in other words, the x-component of the spin for an interaction between two Ir ions bonded by an x-bond, and so on). (Figure generated with VESTA.[10])

The K-H model can also be expressed more succinctly in matrix form:

$$H = \sum_{\alpha=x,y,z} \sum_{\alpha-bonds} \sigma_j \bullet \mathbf{J}_\alpha \bullet \sigma_k ,$$

where the matrices $\mathbf{J}_\alpha$ are:

$$\mathbf{J}_x = \begin{bmatrix} J+K & 0 & 0 \\ 0 & J & 0 \\ 0 & 0 & J \end{bmatrix}, \ \mathbf{J}_y = \begin{bmatrix} J & 0 & 0 \\ 0 & J+K & 0 \\ 0 & 0 & J \end{bmatrix}, \ \mathbf{J}_z = \begin{bmatrix} J & 0 & 0 \\ 0 & J & 0 \\ 0 & 0 & J+K \end{bmatrix}.$$

The K-H model inspired hope that either the ground state of Na_2IrO_3 was a QSL, or that Na_2IrO_3 might be able to be manipulated into being a QSL. Unfortunately, experiments indicate that the K-H model may be insufficient to describe Na_2IrO_3. While the K-H model predicts a magnetic ground state that is either Néel AF (each spin pointing in the opposite direction of the three nearest neighbor spins), stripy AF (each spin pointing the same direction as one of its three nearest neighbors, forming a stripy pattern), or QSL, the experimentally determined magnetic order of Na_2IrO_3 is zigzag AF (each spin pointing the same direction as two of its three nearest neighbors, forming a zigzag pattern).[3, 4]

Several theories have been proposed to explain why Na_2IrO_3 has this zigzag order. Most of these theories are variations on the K-H model. One theory states that zigzag magnetic order can be stabilized if the Kitaev and Heisenberg terms have the opposite sign as originally suggested.[13] Another says it can be stabilized by considering next- and next-next-nearest (in-plane) neighbor Heisenberg terms in addition to nearest neighbor terms.[14]

$$H = \sum_{NN} \sigma_j \bullet \mathbf{J}_{\boldsymbol{\alpha}} \bullet \sigma_k + J_2 \sum_{NNN} \sigma_j \bullet \sigma_k + J_3 \sum_{NNNN} \sigma_j \bullet \sigma_k.$$

Further contention surrounds the fact that the insulating nature of Na_2IrO_3 is still not fully understood. According to naïve, non-relativistic band theory, Na_2IrO_3 should be a conductor, with five of six t_{2g} orbitals filled. Yet experimentally, it is an insulator, with a band gap of around 340 meV.[15] There is debate over what role the Hubbard repulsion (U) and SOC play regarding this insulating behavior, and disagreement over whether Na_2IrO_3 is a Mott insulator (where the insulating behavior originates from

electron-electron repulsive Coulomb energy), a Slater insulator (where the insulating behavior originates from long-range magnetic order), or if the insulating behavior has a separate origin.[16-18]

Other Kitaev candidate materials have many characteristics in common with Na_2IrO_3. In α-$RuCl_3$, the layered honeycomb structure is preserved, with Ru^{3+} taking the place of Ir^{4+}, and Cl^- taking the place of O^{2-}. α-$RuCl_3$ holds a couple of advantages over Na_2IrO_3; the Ru-Cl-Ru bonds are closer to 90° than the Ir-O-Ir bonds, and α-$RuCl_3$ has no equivalent to the intercalated layer of sodium, which complicates the picture.[19] On the other hand, the SOC is smaller in the 4*d* α-$RuCl_3$ than the 5*d* Na_2IrO_3.

Here, we model the electronic and magnetic structures of various Kitaev candidate materials, and using recently developed methods in computational materials science, we investigate spin interactions. In modeling these materials, we used Vienna Ab initio Simulation Package (VASP) to perform DFT(+*U*+SOC) calculations.[20-24] In addition to DFT, we used adiabatic spin-constrained DFT (aSC DFT), which allows for fixing the spin moments in specified directions and with specified magnitudes.

Adiabatic Spin-Constrained DFT (aSC DFT)

In DFT, the ground state electron density $n(r)$ of a many-body system is approximated as the electron density that minimizes the Kohn-Sham energy functional $E^{KS}[n(r)]$:

$$E^{KS}[n(r)] = \int V_{ext}(r)\, n(r) dr + E_H[n(r)] + E_{XC}[n(r)] + T_S[n(r)],$$

where $V_{ext}(r)$ is the external potential, $E_H[n(r)]$ and $E_{XC}[n(r)]$ are the Hartree and exchange-correlation energy functionals, and $T_S[n(r)]$ is the Kohn-Sham kinetic energy

functional.[25, 26] Normally, the minimum Kohn-Sham energy corresponds to the ground state spin structure of the material. We wanted to derive spin-spin interactions, however, which requires the ability to explore the energy landscapes of materials as a function of spin direction. This challenge can be met using aSC DFT, a modified version of DFT that allows for fixing the direction and magnitudes of spins during minimization.

For aSC DFT, spins are fixed by adding a Lagrangian term to the energy functional:

$$E[n(r), s(R)] = E^{KS}[n(r)] + \sum_{a=1}^{N} B_a \cdot (\langle \sigma_a \rangle - s_a),$$

thereby minimizing the energy with the constraint $\langle \sigma_a \rangle = s_a$, where s_a are the desired spin moments, σ_a are the calculated moments, R are the ionic coordinates, and B_a, the Lagrangian multipliers, are equal to the local magnetic fields required to counteract the tendency of DFT to move the spins away from the desired arrangement and towards the ground state arrangement. We performed Compressive Sensing (CS) on results from aSC DFT, to find the spin exchange interactions of Kitaev candidate materials.

Compressive Sensing Spin Dynamics (CSSD)

CS is a signal processing technique for reconstructing a sparse signal based on a limited sampling. If a signal x is known to be sparse in some basis, then there exists some vector $y = Ax$ such that the length of y is significantly smaller than the length of x, and all the information in x is captured in y. In CS, y is measured directly, with each measurement corresponding to linear combinations of the signals in x (in accordance with the *measurement matrix* A). Since x is longer than y, an infinite number of possible solutions to x exist, but (assuming x is sparse) with overwhelming probability, the "true"

values for x can be found by minimizing the ℓ_1 norm of x, subject to the constraint $y = Ax$. If the data contain noise, the ℓ_1 norm can be minimized subject to a constraint that penalizes inaccurate solutions, such as via an ℓ_2 norm for the difference between y and Ax.

In CSSD, the desired signals ("x" above) are the spin interaction terms, captured by J. The measurements ("y") are the local magnetic fields, B (consisting of the various B_a), found via aSC DFT. The measurement matrix, A, can be found by Taylor expanding the energy with respect to the spins:

$$E = \sum_a \sum_{i=1}^{3} J_{a,i} s_{a,i} + \frac{1}{2} \sum_{a,b} \sum_{i,j=1}^{3} J_{ab,ij} s_{a,i} s_{b,j} + \cdots,$$

where a and b are the sites of the spins, i and j are the Cartesian directions, and $s_{a,i}$ and $s_{b,j}$ are the components of the spins on site a and b in the directions of i and j, respectively. Since $B_a = -\partial E / \partial s_a$, we are left with (assuming the derivative is taken at perturbations about the local equilibrium and the first term disappears):

$$B_a = -\sum_b J_{ab} s_b - \cdots,$$

in which J_{ab} is the interaction matrix between the spins at a and b. By running aSC DFT on multiple spin configurations perturbed from a local equilibrium, a set of L linear equations can be found, such that we have $B = AJ$, where the measurement matrix is:

$$A = \begin{bmatrix} -s_b^1 - \cdots \\ \vdots \\ -s_b^L - \cdots \end{bmatrix},$$

where each row corresponds to a different local magnetic field on a particular site, and the superscripts refer to different spin configurations.

The interaction terms are then calculated by:

$$J^{CSSD} = \arg\min_J \left(\|J\|_1 + \frac{\mu}{2} \|B - AJ\|_2^2 \right),$$

where the first and second terms are the ℓ_1 and ℓ_2 norms, and μ is a parameter for trading off between these two. Lower values of μ produce sparser solutions, and thus are prone to under-fitting, while higher values of μ are prone to over-fitting. The fit can be checked by leaving out a portion of the data and conducting cross-validation.

Results

Na_2IrO_3 Electronic and Magnetic Structure

In order to determine the roles that electronic correlations and SOC play in the electronic behavior of Na_2IrO_3, we compared results between LSDA+*U*+SOC and calculations performed without *U* and/or SOC. We used the on-site Coulomb interaction according to the approach by Dudarev *et al*, which is dependent not on *U* in and of itself, but instead on $U_{eff} = U - J$, where *J* represents the effective on-site exchange interaction.[27] Unless where otherwise noted, we used a *k*-point grid of 6x4x6, an energy cutoff of 10^{-5} eV for electronic convergence, a cutoff for ionic convergence of all forces being under 0.01 eV/Å, and PBE-PAW potentials (with the hard version of the oxygen potential).[28]

As a test to ensure that these parameters were appropriate, we performed several select calculations, increasing the *k*-mesh to 8x6x8 and decreasing both the electronic and ionic convergence cutoffs by a factor of 10. None of these changes appreciably changed any results.

We ran DFT with four separate magnetic structures: ferromagnetic, Néel antiferromagnetic, stripy antiferromagnetic, and zigzag antiferromagnetic (Figure 7).

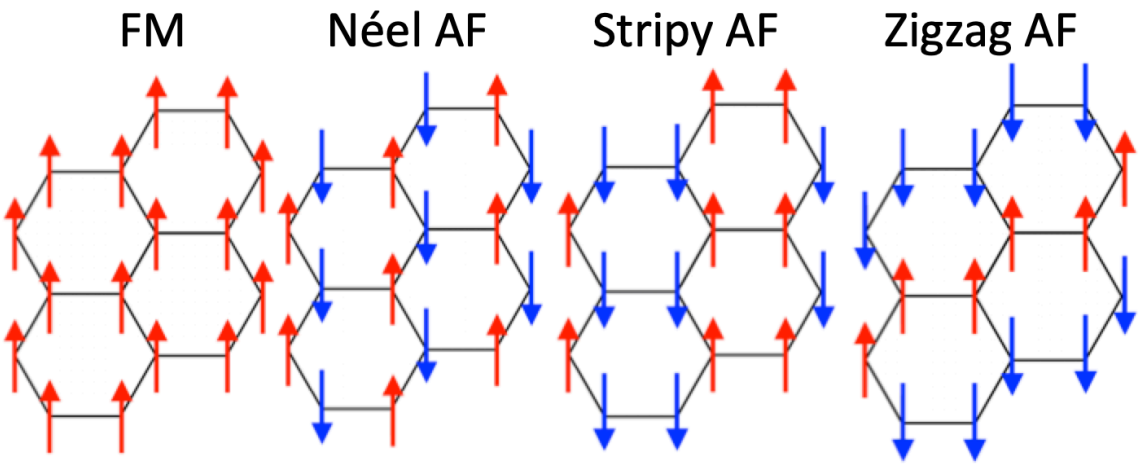

Figure 7: The four magnetic orders that we tested. From left to right, these orders are FM, Néel AF, stripy AF, and zigzag AF.

Curiously, our initial results from LSDA+U often yielded significant changes in the band gap and converged energy when parameters were changed in ways that should have been inconsequential. Since DFT+U is known to exhibit local energy minima in orbital occupancies, the most likely explanation is that different local minima were found. To examine this effect further, we perturbed the original Na_2IrO_3 structure in 20 different ways, by displacing each atom in a random direction very slightly (less than 0.01 Å). We then relaxed all 20 of these different starting structures, and also the original structure, each under all four magnetic orders (with all other parameters the same), using an unrealistically high U (U_{eff} = 4.7 eV) to increase the number of local minima found. In total, of these 84 relaxations performed, 16 "unique" solutions were found, where two solutions were determined to be unique if they had different magnetic order or a difference in their relaxed energy (or band gap) greater than 1 meV/Ir (0.05 eV).

These 16 solutions were then used as starting points for further LSDA+U calculations with lower U (at U_{eff} = 3 eV), each with the four different magnetic structures. The output ionic positions from the U_{eff} = 4.7 eV calculations were used as the input ionic positions at U_{eff} = 3 eV, and the output charge densities were used as input charge densities for calculations that continued with the same magnetic order. Unique solutions found at U_{eff} = 3 eV were then continued at U_{eff} = 2.75 eV (under the same magnetic order). This process of continuing unique solutions after decreasing U_{eff} by 0.25 eV was carried out until a U_{eff} of 0.5 eV. There is some debate in the literature about the correct value for U, but it is generally accepted to be somewhere in the range of 1 eV to 3 eV, and J is usually assumed to be around 0.5 eV.[4, 29]

While the number of distinct solutions found for each magnetic order decreased as U_{eff} decreased, there remained several, even at low U_{eff}. Of note, the difference in energies between solutions of the same magnetic order was often greater than the difference in energies between solutions of different magnetic orders (Figure 8). For comparing the different magnetic orders, it is therefore important to ensure that the solution for each magnetic order truly is the ground state solution for that magnetic order.

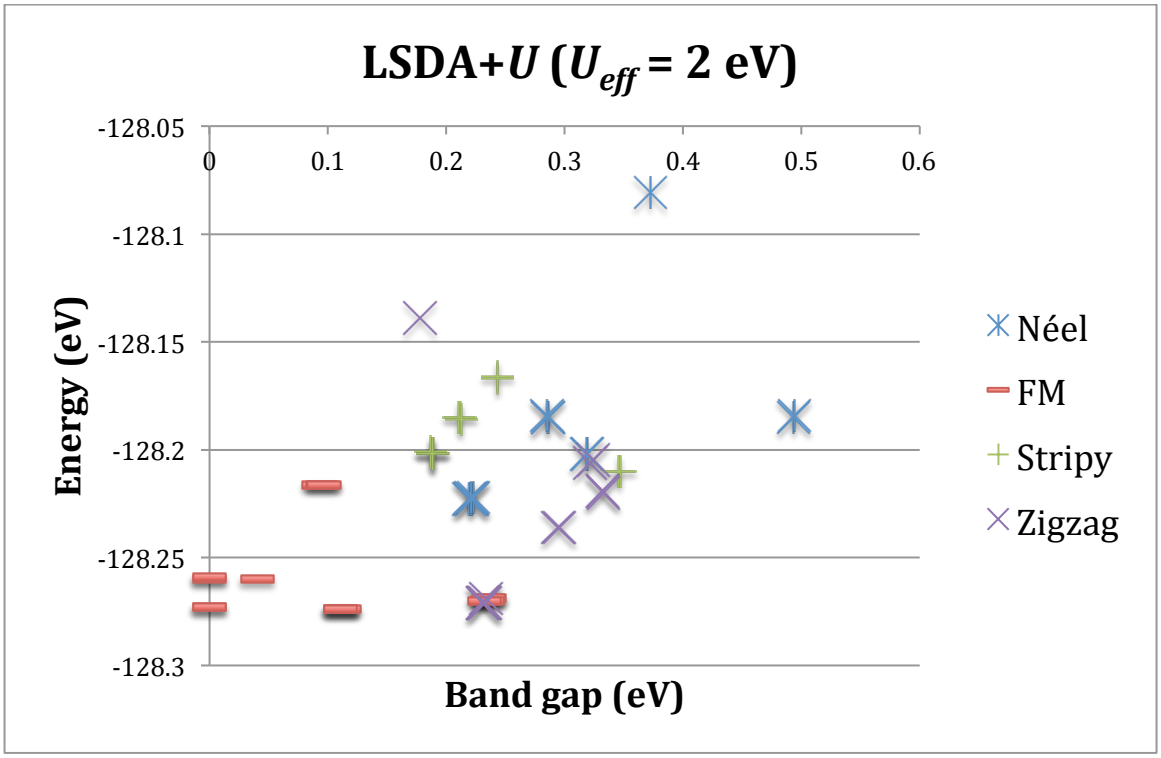

Figure 8: The energy and band gap for structures of the four magnetic orders, after convergence using LSDA+U with U_{eff} = 2 eV. The spread of different solutions for the same magnetic order implies multiple local energy minima found. Note that the difference in energy between solutions of the same magnetic order is often larger than that between different magentic orders.

Inspection showed that different solutions typically correspond to different occupancies of Ir 5*d* orbitals, while calculations that resulted in the same solution typically correspond to almost identical occupancies of these orbitals. This result potentially explains some contradictions and other peculiar results in the literature surrounding Na_2IrO_3. For instance, different papers using DFT have found different angles of orientation for the magnetic spins.[3, 30] Separately, other DFT calculations often indicate that very small structural changes in Na_2IrO_3 can lead to surprisingly large differences in properties.[31] Both of these findings could be explained by some of the calculations resulting in solutions that are not in fact the ground state, but instead metastable states. A similar phenomenon has been observed in 3*d* and 5*f* materials with

highly localized orbitals, but we were somewhat surprised to find it appearing in a 5*d* material here.[32]

Comparing the lowest energy solution for each magnetic order at each value of U_{eff} shows that the lowest energy order is FM for all values of U_{eff} that are less than 2 eV (Figure 9: left). Above $U_{eff} = 2$ eV, the zigzag order becomes the lowest energy solution, but the FM order is energetically competitive (it is always within 3 meV per Ir).

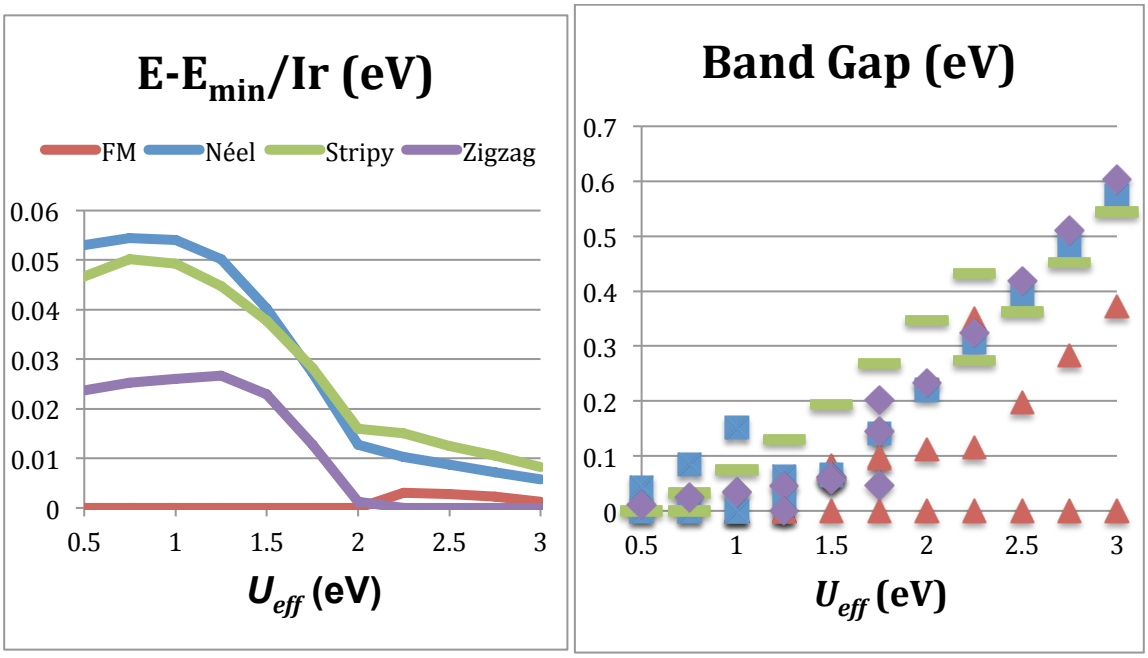

Figure 9: LSDA+*U* results. Left- The lowest energy solution for each magnetic order at each step of U_{eff}, compared to the lowest energy solution of all the magnetic orders at that step. Right- The corresponding band gaps for those lowest energy solutions. At some steps of U_{eff}, certain magnetic orders have multiple values for the band gap, due to multiple solutions with the same lowest energy (or within 3 meV per Ir) but different band gaps.

Unfortunately, comparing band gaps of different magnetic orders was more difficult than comparing the energies (Figure 9: right). Often, multiple solutions of the same magnetic order had the same lowest energy (or within 3 meV per Ir), but quite different band gaps. This difference in band gaps for the same magnetic order was even

occasionally greater than 0.3 eV. The two lowest energy magnetic orders – zigzag and FM – generally had no band gap or a very small band gap when $U_{eff} \leq 1.25$ eV, but did have a band gap above this value (or in the case of FM, at least one solution per value of U_{eff} had a band gap).

For LSDA+U+SOC, we varied U_{eff} from 0.5 eV to 2 eV, in increments of 0.5 eV, starting at 2 eV and continuing unique solutions at lower U_{eff} as before. For the calculations at $U_{eff} = 2$ eV, for each magnetic order, the input atomic positions were the unique solutions found under LSDA+U at 2 eV with the same magnetic order. We relaxed each of these solutions three separate times – each with the magnetic moments initially pointing along a different axis of the unit cell (though these moments were allowed to move during relaxation). We found fewer unique solutions with the introduction of SOC, though the differences in energy between solutions of the same magnetic order were again often greater than the differences in energy of solutions of different magnetic orders. At each value of U_{eff}, the lowest energy solution was of zigzag order, and this solution was always at least 3 meV per Ir lower energy than the next lowest energy solution from a different magnetic order (Figure 10: left). This finding is consistent with experimental research that has demonstrated Na_2IrO_3 exhibits zigzag magnetic order.[3, 4] Fortunately, with SOC added, the lowest energy solution for each magnetic order corresponds to a single band gap (Figure 10: right). Predictably, adding in SOC increases the band gaps considerably.

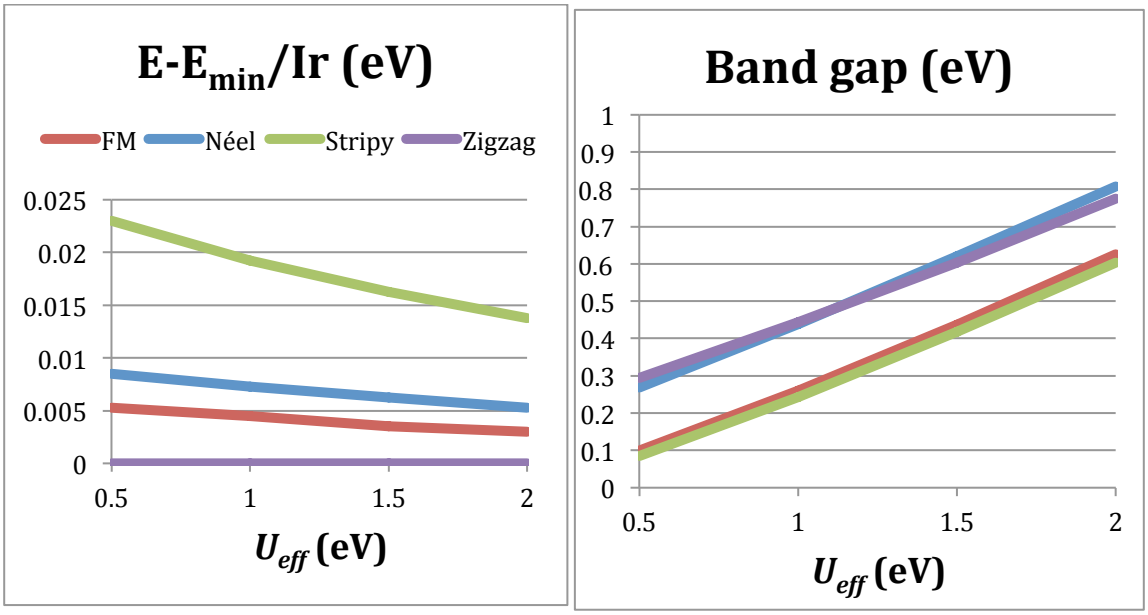

Figure 10: LSDA+*U*+SOC results. Left- The lowest energy solution for each magnetic order at each step of U_{eff}, compared to the lowest energy solution of all the magnetic orders at that step. Right- The corresponding band gaps for those lowest energy solutions.

Experimentally, the band gap of Na_2IrO_3 has been found to be 0.34 eV.[15] Through interpolation, this corresponds to U_{eff} = 0.65 eV. Indeed, when we performed LSDA+*U*+SOC with U_{eff} = 0.65, we found a band gap of 0.339 eV for the lowest energy solution of zigzag magnetic order. Since $J \sim 0.5$, this corresponds to a $U \sim 1.15$ eV.

We used this value of U_{eff} to investigate the effects of *U* and SOC on the band structure. To do this, we performed band structure calculations of the lowest energy solutions for the zigzag order with LSDA+*U* and LSDA+*U*+SOC, using U_{eff} = 0.65. We also found the lowest energy solutions for the zigzag order with LSDA and LSDA+SOC (without *U*), and we calculated the band structure of those as well. We determined all *k*-paths with the software AFLOW.[33]

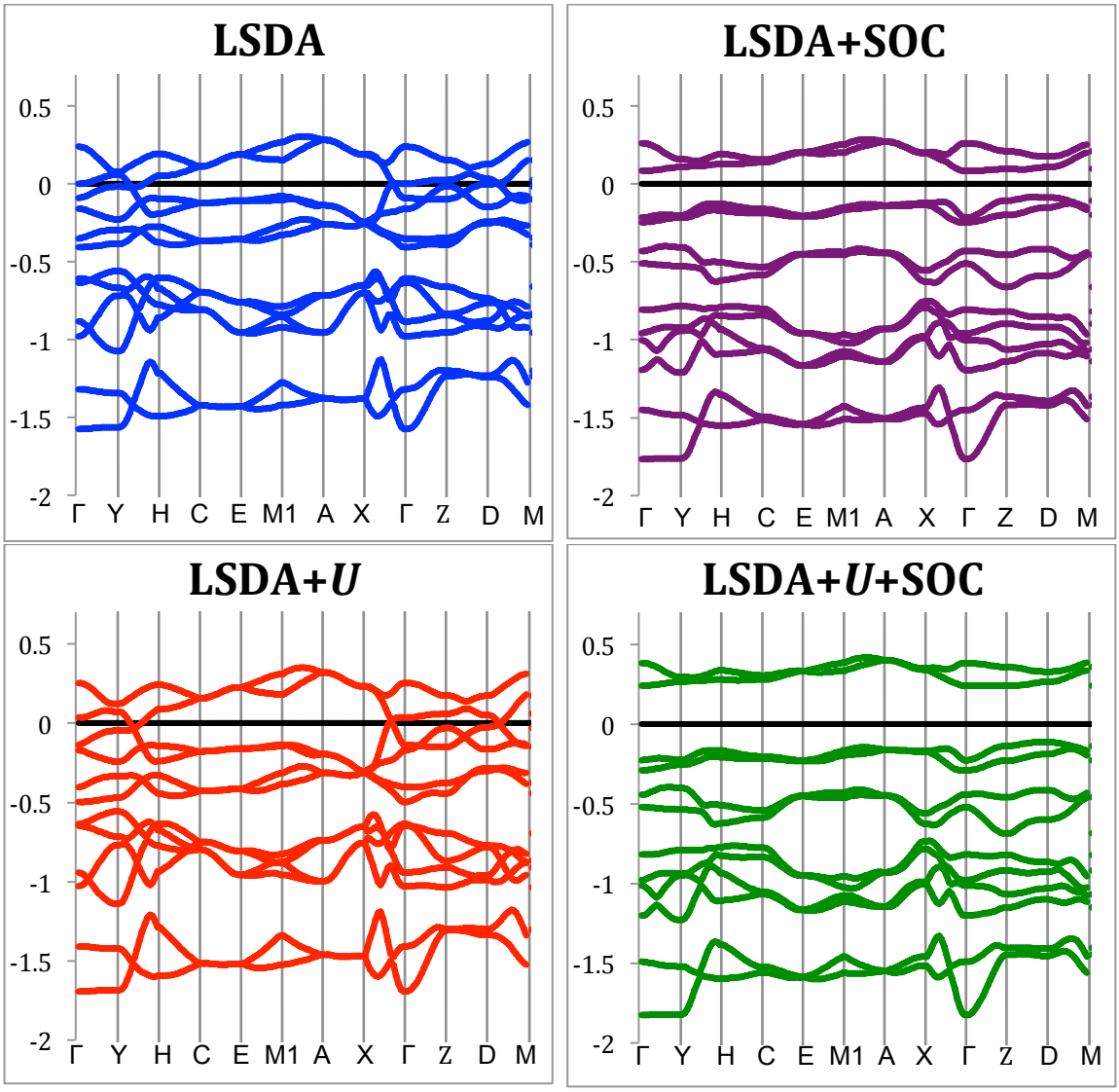

Figure 11: Band structures of the t_{2g} orbitals in the zigzag order, using LSDA (top left), LSDA+SOC (top right), LSDA+*U* (bottom left), and LSDA+*U*+SOC (bottom right). The SOC appears necessary and sufficient to open the band gap, and *U* increases this band gap.

Comparing these band structures, the effects of *U* appear quite small, while the effects of SOC appear much larger (Figure 11). Qualitatively, band structures for LSDA and LSDA+*U* are almost identical, while the only major difference between that of LSDA+SOC and LSDA+*U*+SOC is that the latter has about twice the band gap of the former. This low importance of *U* casts doubt on the commonly held idea that Na_2IrO_3 is

a Mott insulator. U is neither necessary nor sufficient for opening up the band gap in the zigzag order, while SOC is both. It should also be noted that both with U_{eff} = 0.65 eV and without U_{eff}, the FM order has lower energy than the zigzag order if SOC is neglected (but not if SOC is included). This FM order also corresponds to no band gap under these parameters. We conclude that Na_2IrO_3 is a spin-orbit induced band-gap insulator.

Na_2IrO_3 and α-$RuCl_3$ Exchange Interactions

To understand the Ir-Ir (Ru-Ru) spin interactions, we performed CSSD with Na_2IrO_3 (α-$RuCl_3$), using the following methodology. First, six relaxations were performed – 3 with FM spins initially pointing in each one of three orthogonal directions (two in-plane and one out-of-plane), and 3 with AF spins initially pointing in each of the same three directions. This step involved using LSDA+SOC (without U) on VASP with electronic cutoffs of 10^{-5} eV and ionic cutoffs of all forces under 0.01 eV/Å.

The lowest energy of these six relaxations was then used as a reference for running further calculations. These further calculations used aSC DFT to fix the magnetic moments in desired directions and with desired magnitudes. Calculations were performed both with a primitive cell (of 2 Ir/Ru per cell) and with a supercell (of 18 Ir/Ru per cell, such that ions had unique nearest, next-nearest, and next-next-nearest in-plane neighbors). In calculations with the primitive cell, both magnetic moment orientations were moved together, while in calculations with the supercell, only one moment was altered, while the other moments were kept in the reference direction (Figure 12).

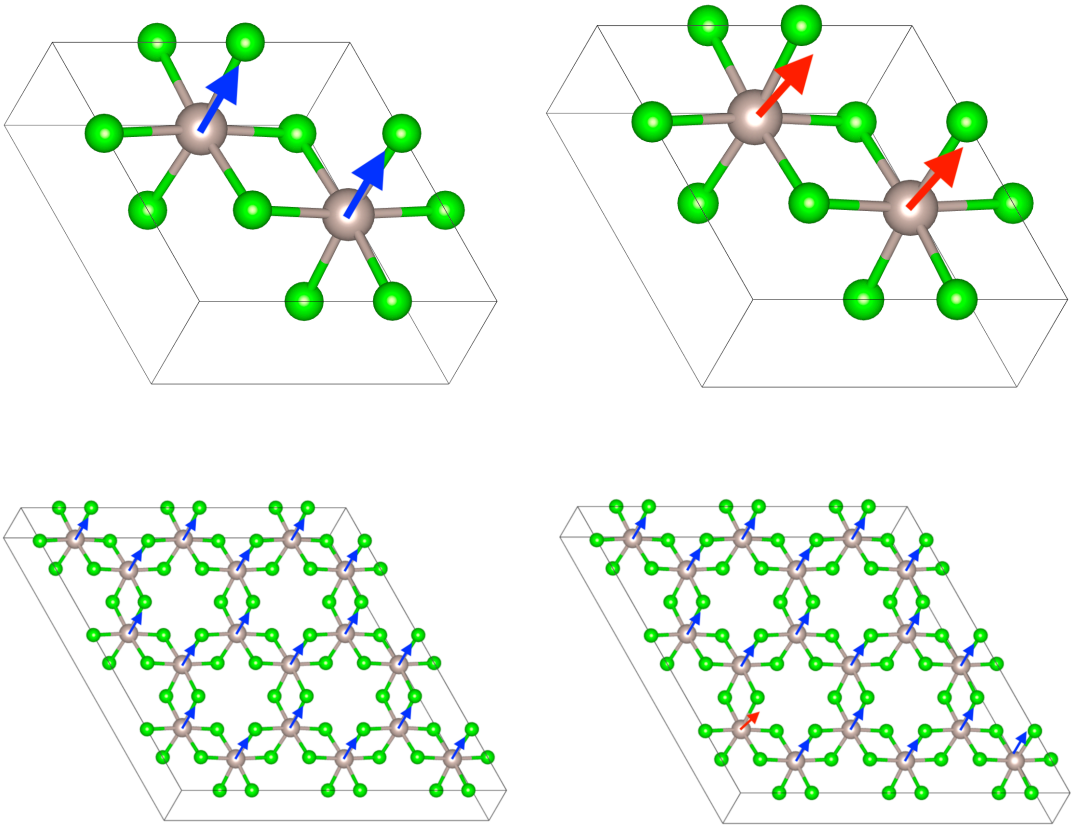

Figure 12: Primitive cells and supercells of α-$RuCl_3$, with magnetic moments. The blue moments are in the reference direction, while the red moments are perturbed. In the primitive cell, all the moments are perturbed simultaneously (and to the same degree). In the supercell, only one moment is perturbed (and all other moments are kept in the reference direction). (Figure generated with VESTA.[10])

One calculation was performed using the primitive cell with all the moments fixed in the reference direction. Calculations were then performed using each of the primitive cell and the supercell, with the relevant moments moved from the reference direction by between ~0.1 μ_B and ~0.2 μ_B in various directions, with 12 calculations total for each of the primitive cell and the supercell. All moments were kept at the same magnitude as in the reference calculation. These calculations were performed to an electronic cutoff of 10^{-7} eV using LSDA+SOC within a modified version of VASP, and ions were not allowed to relax. The results of these calculations were used for CSSD.

We used LSDA+SOC without U because the code we were using for fixing the spins did not allow for simultaneously fixing the spins and enabling U, but we believe not including U in these calculations was appropriate, for a few reasons. First, as demonstrated in the section "Na_2IrO_3 Electronic and Magnetic Structure," LSDA+SOC gave qualitatively similar results to LSDA+U+SOC, with U simply increasing the band gap. Second, as demonstrated in the same section, the inclusion of U increases the chances of a local (though not global) energy minimum being found, and inclusion of such results here could negatively affect CSSD (by, for instance, implying that moving the magnetic moment in one direction had different results than it actually would). Third, the way DFT+U employs U is not in accordance with fundamental physics, but instead as an empirical fix to correct for underestimating the band gap; there's no guarantee that this same fix would improve the results here.

The last step in performing CSSD was to perform CS on the data we received from the above calculations. Here, the magnetic fields required to obtain the desired magnetic moments were used to determine the (in-plane) nearest, next-nearest, and next-next-nearest neighbor spin Hamiltonians. A μ of 10^{-7} was used for these calculations. Cross validation was performed to check fit, with relative errors calculated as follows: five times, 9% of the data were left out to check against what would be predicted from the other 91%, and the errors of those five times were averaged.

Na_2IrO_3

CSSD with Na_2IrO_3 produced the following interaction matrices with 15% relative predictive error:

Nearest neighbors (interaction terms are in meV/μ_B^2):

$$\mathbf{J_x} = \begin{bmatrix} 45 & -7 & 6 \\ -7 & 61 & 8 \\ 6 & 8 & 57 \end{bmatrix}, \quad \mathbf{J_y} = \begin{bmatrix} 61 & -7 & -8 \\ -7 & 45 & -6 \\ -8 & -6 & 57 \end{bmatrix}, \quad \mathbf{J_z} = \begin{bmatrix} 50 & 4 & 10 \\ 4 & 50 & -10 \\ 10 & -10 & 31 \end{bmatrix}.$$

Note that $\mathbf{J_y}$ here is simply related to $\mathbf{J_x}$ by symmetry. As expected, the dominant values are along the diagonals, corresponding to the values for J_1 and $J_1 + K$; the off-diagonal Γ terms are much smaller. There are three unique (i.e., not simply related by symmetry operations) terms for J_1, and two unique terms for $J_1 + K$. The average value of J_1 is therefore (61 + 57 + 50)/3 = 56 meV/μ_B^2, while the average value of $J_1 + K$ is (45 + 31)/2 = 38 meV/μ_B^2. K therefore has an approximate value of: 38 – 56 = -18 meV/μ_B^2, or around one third of the magnitude of J_1.

Second-nearest neighbors (in meV/μ_B^2):

$$\mathbf{J_{2,1}} = \begin{bmatrix} 25 & 0 & 2 \\ 1 & 29 & -1 \\ 3 & 0 & 26 \end{bmatrix}, \quad \mathbf{J_{2,2}} = \begin{bmatrix} 24 & -3 & 2 \\ -2 & 24 & -1 \\ 1 & -2 & 28 \end{bmatrix}.$$

Additional second-nearest neighbor interaction matrices are related to these via symmetry (as is also true for the third-nearest neighbor matrices – for subsequent results, we also only report the unique matrices for the second- and third- neighbor interactions). Here, the only large terms are the diagonal J_2 terms, implying a value of approximately 26 meV/μ_B^2, or around half of J_1.

Third-nearest neighbors (in meV/μ_B^2):

$$\mathbf{J_{3,1}} = \begin{bmatrix} 2 & -11 & 10 \\ -11 & 2 & -10 \\ 10 & -10 & 0 \end{bmatrix}, \quad \mathbf{J_{3,2}} = \begin{bmatrix} -1 & -13 & 11 \\ -13 & 4 & -6 \\ 11 & -6 & 1 \end{bmatrix}.$$

The J_3 terms here are negligible, at an average value of approximately 1 meV/μ_B^2. The off-diagonal terms here are larger in magnitude, but they are still much smaller than the magnitudes for J_1, J_2, and K.

The overall picture of this material is of three interactions: J_1, J_2 of around one-half of J_1, and K at a "disappointing" one-third of J_1.

We decided to test whether these results were robust with respect to the reference magnetic structure. While Na_2IrO_3 is zigzag magnetic structure, a zigzag supercell that allowed for examining third-nearest neighbors would have had to be much larger than the supercell used here, and beyond reasonable computational resources. We instead decided to perform CSSD on a dataset that included both AF and FM calculations. In performing the AF calculations, we used the same relaxed structure as for the FM calculations above, as well as the same magnetic-moment axis and magnitudes, so that the only change was turning the moments antiferromagnetic. We included the same FM data as above, and for each FM calculation we included a corresponding AF calculation, with all other parameters the same.

CSSD with this combined dataset yielded the following Hamiltonians with 4.4% relative error (in meV/μ_B^2):

$$\mathbf{J_x} = \begin{bmatrix} 50 & 5 & -4 \\ 5 & 46 & -5 \\ -4 & -5 & 44 \end{bmatrix}, \quad \mathbf{J_y} = \begin{bmatrix} 46 & 5 & 5 \\ 5 & 50 & 4 \\ 5 & 4 & 44 \end{bmatrix}, \quad \mathbf{J_z} = \begin{bmatrix} 40 & -5 & -1 \\ -5 & 40 & 1 \\ -1 & 1 & 44 \end{bmatrix}.$$

Second-nearest neighbors (in meV/μ_B^2):

$$\mathbf{J_{2,1}} = \begin{bmatrix} 30 & -4 & 1 \\ -3 & 33 & -3 \\ 1 & -2 & 25 \end{bmatrix}, \quad \mathbf{J_{2,2}} = \begin{bmatrix} 28 & -2 & 5 \\ -3 & 28 & -3 \\ 3 & -5 & 26 \end{bmatrix}.$$

Third-nearest neighbors (in meV/μ_B^2):

$$\mathbf{J_{3,1}} = \begin{bmatrix} 3 & -4 & 2 \\ -4 & 3 & -2 \\ 2 & -2 & -4 \end{bmatrix}, \quad \mathbf{J_{3,2}} = \begin{bmatrix} -2 & -5 & 3 \\ -5 & 5 & -1 \\ 3 & -1 & 3 \end{bmatrix}.$$

These results are for the most part similar to the FM results. The largest term is still J_1, and the value of J_2 is still around half of that. J_3 and the off-diagonal terms are also still very small. The only significant difference is that K has changed from -18 to 3 meV/μ_B^2, in other words falling from a small factor to a negligible one. The actual situation with Na_2IrO_3 may be somewhere between these two scenarios, since in the zigzag magnetic structure, each spin is ferromagnetic with two of its three nearest neighbors. Regardless, the Kitaev term appears to be quite small. Inducing the Kitaev QSL state requires a K of at least 8 times J_1, or a K:J_1 ratio about 25 times larger than the more "generous" result found with just our FM dataset.

Since inclusion of AF data along with the FM data did not significantly alter the results, we decided to simply use the magnetic structure of lowest energy for subsequent CSSD calculations.

α-RuCl₃

CSSD with α-$RuCl_3$ produced the following Hamiltonians with 13% relative predictive error:

Nearest neighbors (in meV/μ_B^2):

$$\mathbf{J_x} = \begin{bmatrix} 49 & 3 & 4 \\ 3 & 51 & -4 \\ 4 & -4 & 43 \end{bmatrix}, \quad \mathbf{J_y} = \begin{bmatrix} 51 & 3 & 4 \\ 3 & 49 & -4 \\ 4 & -4 & 43 \end{bmatrix}, \quad \mathbf{J_z} = \begin{bmatrix} 59 & 4 & 6 \\ 4 & 59 & -6 \\ 6 & -6 & 42 \end{bmatrix}.$$

Second-nearest neighbors (in meV/μ_B^2):

$$\mathbf{J_{2,1}} = \begin{bmatrix} 28 & 0 & -3 \\ 0 & 28 & 3 \\ -2 & 3 & 33 \end{bmatrix}, \quad \mathbf{J_{2,2}} = \begin{bmatrix} 29 & -2 & -3 \\ -1 & 30 & 2 \\ -2 & 3 & 34 \end{bmatrix}, \quad \mathbf{J_{2,3}} = \begin{bmatrix} 29 & -1 & -3 \\ 0 & 30 & 3 \\ -2 & 4 & 33 \end{bmatrix}.$$

Third-nearest neighbors (in meV/μ_B^2):

$$\mathbf{J_{3,1}} = \begin{bmatrix} 31 & 1 & 1 \\ 1 & 31 & -1 \\ 1 & -1 & 29 \end{bmatrix}, \quad \mathbf{J_{3,2}} = \begin{bmatrix} 31 & 2 & 1 \\ 2 & 31 & -1 \\ 1 & -1 & 27 \end{bmatrix}.$$

These data almost perfectly fit a Heisenberg J_1-J_2-J_3 model. Using a similar method as above, we find the average J_1 = 51 meV/μ_B^2, K = -6 meV/μ_B^2, J_2 = J_3 = 30 meV/μ_B^2. K would have to increase by over a factor of 60 relative to J_1 here to reach a Kitaev QSL state.

If we ignore the K terms (which are quite small for these materials), as well as further anisotropy, we can plot these structures on a classical J_1-J_2-J_3 Heisenberg phase diagram (Figure 13).[34]

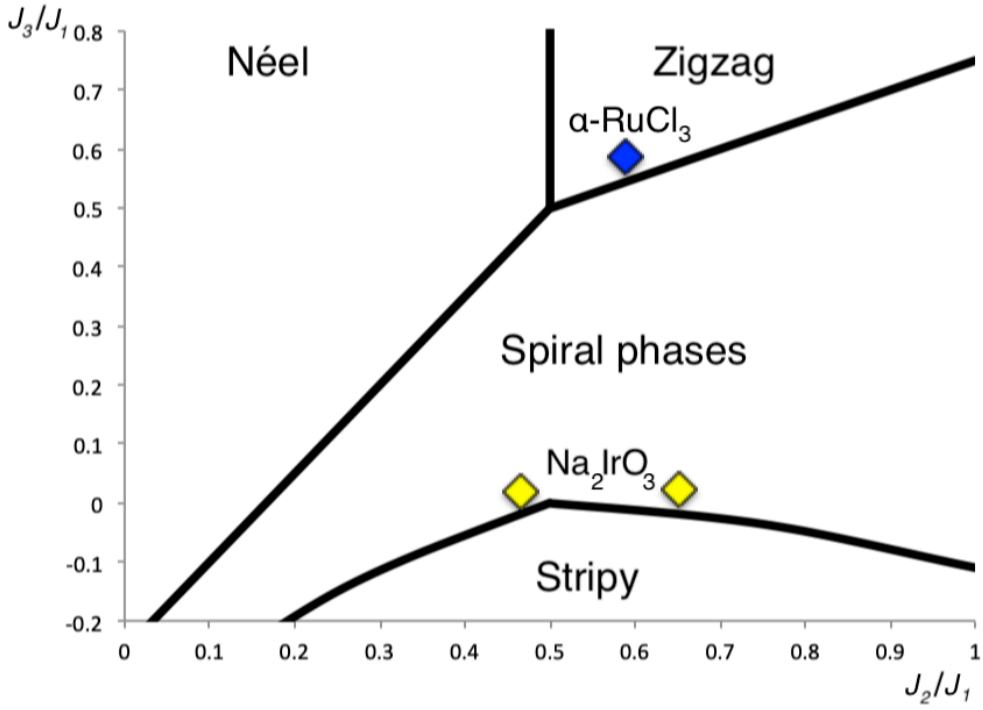

Figure 13: α-$RuCl_3$ and Na_2IrO_3 plotted on a classical J_1-J_2-J_3 Heisenberg phase diagram.

This J_1-J_2-J_3 model explains α-$RuCl_3$ well, as it has zigzag magnetic order. It also possibly explains another finding about α-$RuCl_3$ – under application of a magnetic field, α-$RuCl_3$ shows evidence of entering a QSL phase.[6] Given α-$RuCl_3$'s position on the phase diagram – very close to the triple point – it is presumably a very frustrated material, and thus it is not particularly surprising that it can be induced to enter a QSL phase (though this QSL phase is not necessarily of Kitaev origin).

Na_2IrO_3 is not as well explained by this model, as its magnetic structure is also zigzag, not spiral as indicated here. This discrepancy can likely be explained by two factors that are not included in the J_1-J_2-J_3 model. First, Na_2IrO_3 has large magnetocrystalline anisotropy. Of our LSDA+U+SOC (U_{eff} = 0.65) calculations, different relaxations of Na_2IrO_3 show zigzag order with different spin axes varying in energy by as much as 6 meV per Ir. This magnetocrystalline anisotropy would favor collinear magnetic phases such as zigzag and stripy over the noncollinear spiral phases. Second, the small Kitaev term may be playing a role. In a K-J_1-J_2-J_3 model, as K grows from zero, the zigzag phase on the J_2/J_1 v J_3/J_1 phase diagram grows down and left, at the expense of the Néel and spiral phases (the stripy phase also grows, though not as much, and in a leftward direction that may be away from where Na_2IrO_3 is on this diagram).[14] We note that while Na_2IrO_3 has a zigzag ground state, Li_2IrO_3, which is isostructural and isoelectronic with Na_2IrO_3, has a spiral ground state.[35] We can only speculate that Na_2IrO_3 may have larger magnetocrystalline anisotropy than Li_2IrO_3, which would conceivably explain this difference.

From CSSD, the major Kitaev candidate materials appear to have large nearest-neighbor Heisenberg interactions, moderately large second-nearest-neighbor Heisenberg

interactions, small Kitaev interactions, and variation from small to moderately large third-nearest-neighbor Heisenberg interactions.

Manipulated Kitaev Candidate Materials

While Na_2IrO_3 and α-$RuCl_3$ may not themselves enable Kitaev QSL states, many proposals have been made for manipulating them into Kitaev QSL states. Here, we examine epitaxial and single layers of Na_2IrO_3, strained Na_2IrO_3, and idealized versions of Na_2IrO_3 and α-$RuCl_3$.

Epitaxial and Single Layers

GaN/Na_2IrO_3

We searched Materials Project for possible substrates for Na_2IrO_3.[36] We settled on GaN for several reasons. First, the lattice mismatch between Na_2IrO_3 and GaN is small; the cross-hexagon distance is 6.26 Å for Na_2IrO_3 and 6.43 Å for GaN. We hypothesized that the slightly larger distance for GaN may even help, as expanding Na_2IrO_3 in-plane may decrease the Heisenberg terms relative to the Kitaev term. Second, GaN is an insulator (3.4 eV band gap). Third, GaN can be grown by MBE, meaning synthesizing GaN/Na_2IrO_3 may be achievable.

We performed DFT calculations on a slab containing four layers of GaN (24 Ga ions) and one double layer of Na_2IrO_3 (one layer of $NaIr_2O_6$ and one layer of Na; 4 Ir ions) (Figure 14). We performed LSDA+U+SOC on the material (with the magnetic structure initialized to zigzag order) with U_{eff} = 0.65 eV. We used a k-mesh of 6x4x1, and

for ionic relaxation, we allowed the ions and cell shape to relax but held the cell volume constant. We set all the other parameters the same as in our Na_2IrO_3 calculations.

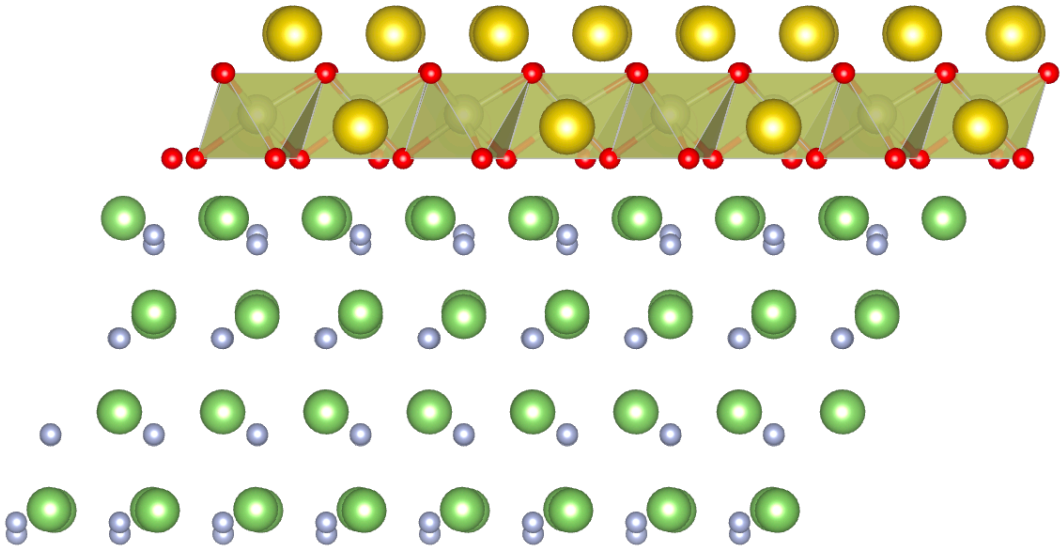

Figure 14: Relaxed GaN/Na_2IrO_3 structure. (Figure generated with VESTA.[10])

Unfortunately, despite GaN and Na_2IrO_3 both being insulators, we found this material to be a conductor. We considered that the insulating behavior may be due to the double-layer of Na_2IrO_3 on the end, and so we repeated this process with just a double-layer of Na_2IrO_3. As expected, this material was also a conductor, though the Na within the $NaIr_2O_6$ layer popped-out of the layer (Figure 15 – left). We additionally ran similar calculations with a double-layer of Na_2IrO_3 held static (ionic relaxation turned off) to assess whether structural changes were causing the conducting behavior, but a similar electronic calculation with this material still revealed conducting behavior (Figure 15 – right). We surmise that growing double-layer thin films of Na_2IrO_3 on a GaN substrate is not a promising avenue to induce a Kitaev QSL. It remains to be seen whether a suitable oxide substrate can be found. The Na layers on both sides of the $NaIr_2O_6$ layer appear to affect the band structure, implying Na_2IrO_3 cannot be cleanly

separated into individual layers without drastically changing the band structure at the Fermi level.

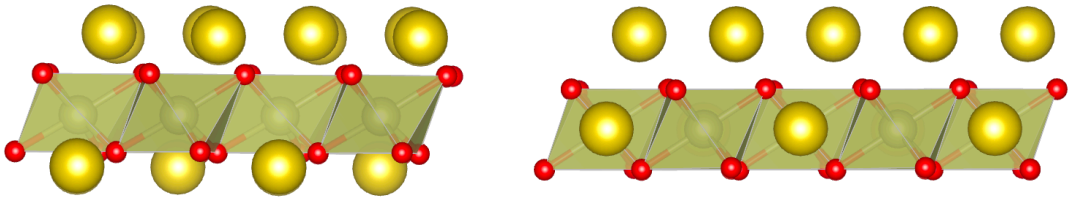

Figure 15: Relaxed (left) and static (right) double layers of Na_2IrO_3. (Figure generated with VESTA.[10])

Strained Na_2IrO_3

It has been suggested that applying strain on Na_2IrO_3 may enable the Kitaev QSL state, for one of two reasons.[37, 38] First, as alluded to in the previous section, an expanded unit cell would mean larger Ir-Ir distances, and therefore smaller Heisenberg interactions.[37] Second, it may be possible to apply strain to coax the Ir-O-Ir angles closer to 90°; this would presumably lead to more destructive interference from the isotropic parts of the Ir-O-Ir interactions and thus smaller Heisenberg interactions.[38] We therefore performed a series of DFT calculations on Na_2IrO_3 at various amounts of strain.

For these calculations, we started with the experimental Na_2IrO_3 unit cell, and produced four more unit cells by simultaneously varying strain in both of the in-plane directions (5% tension, 10% tension, 5% compression, and 10% compression) while scaling all of the ion positions. We kept the out-of-plane distances constant; while most materials have positive Poisson's ratios (often of ~0.3), layered materials don't follow a clear pattern regarding Poisson's ratios in their out-of-plane directions, and instead can have Poisson's ratios in this direction that are positive, negative, or near zero, so we felt that an assumption of zero was a good prior.[39]

For each of these five unit cells (the four strained and the one unstrained), we performed LSDA+U+SOC (U_{eff} = 0.65 eV) while keeping the unit cell shapes and volumes constant during ionic relaxation, and all other parameters at our default settings. For each structure, we performed 12 calculations – 3 for each magnetic order (with spins initialized along different unit cell axes for each of the 3 calculations).

While in the unstrained structure, zigzag magnetic order has the lowest energy, at extreme tension and compression, the FM order has the lowest energy, and the difference between these two decreases at the more moderate strains as well (Figure 16 – left). Interestingly, the band gap also decreases as the strain increases (again, in both directions) (Figure 16 – right).

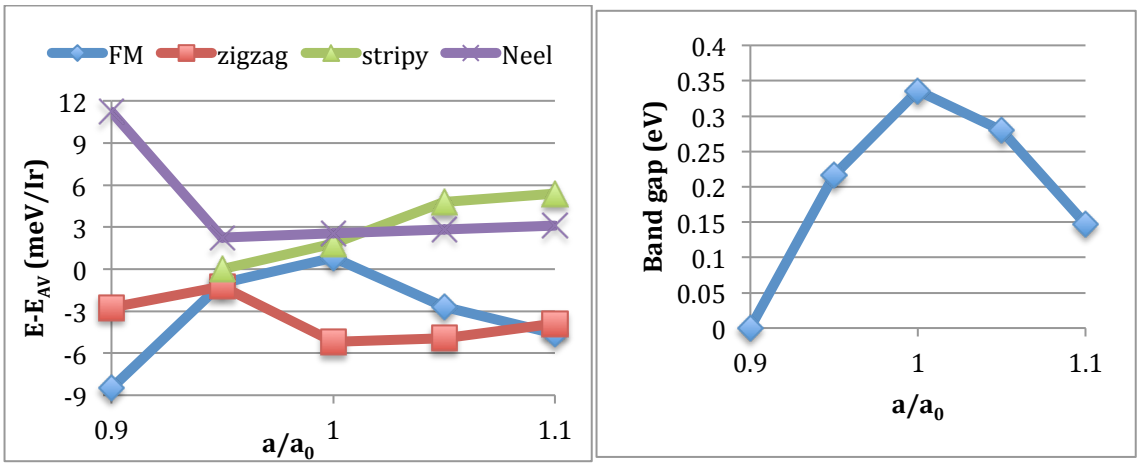

Figure 16: Left – relative energy of the magnetic structures at various strain. Right – band gap of the lowest energy magnetic structure at each level of strain.

Under an assumption of a K-J_1-J_2-J_3 model, as K increases relative to J_1, the zigzag and stripy phases are expected to grow on the phase diagram at the expense of the Néel phase.[14] In this situation, smaller J_2 and J_3 (also thought to be a requirement for the Kitaev QSL) would favor a stripy phase over zigzag. As tension is applied here, however, both the zigzag and stripy phases increase in energy relative to the Néel phase, while the

FM phase decreases in energy relative to all three (which is not expected as Kitaev QSL is approached). Under 5% compression, the stripy phase does decrease in energy, but it never decreases below the zigzag or FM phase, and the zigzag structure here increases in energy compared to FM. All three of these phases have relatively similar energies, implying a large amount of frustration, and conflicting evidence regarding hopes for achieving the QSL phase via elastic strain.

Examining the Ir-O-Ir angles suggests an explanation for this phenomenon. The angles grow under tension and shrink under compression, with a close-to-ideal 94° at 5% compression (Figure 17). As explained in the introductory section on Na_2IrO_3, ideal IrO_6 octahedra are expected to show strongest Kitaev-like couplings relative to Heisenberg interactions, as the isotropic portion of Ir-O-Ir hopping destructively interferes at an Ir-O-Ir angle of 90°.

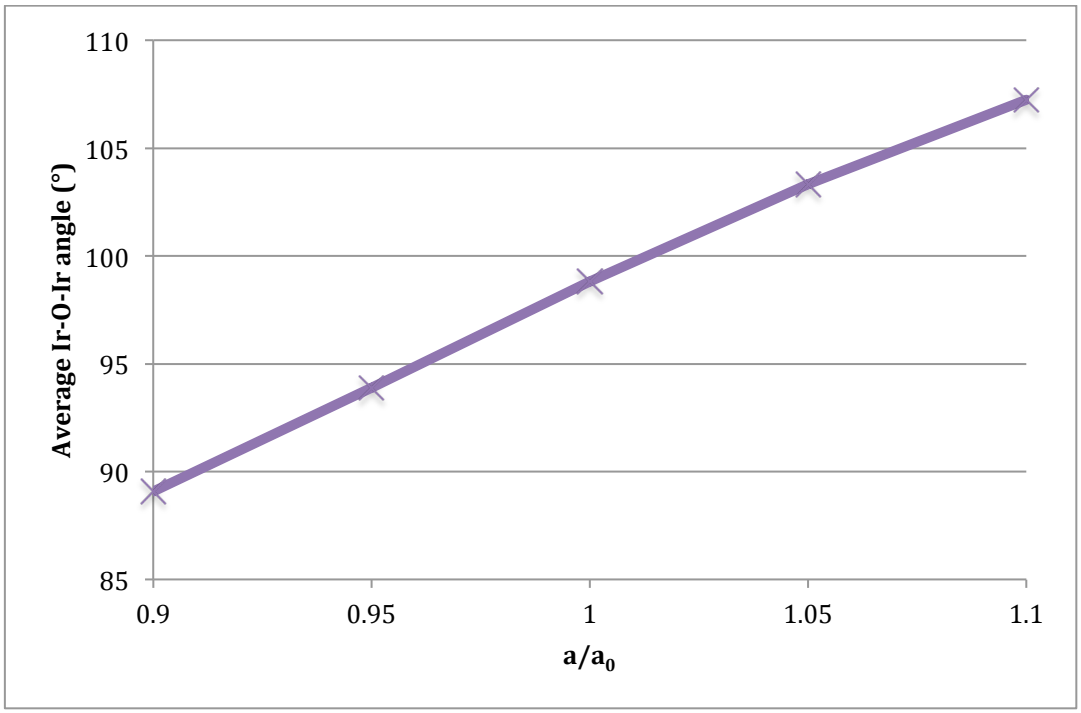

Figure 17: Ir-O-Ir angles in Na_2IrO_3 increase approximately linearly with in-plane lattice constants.

Idealized Na_2IrO_3 and α-$RuCl_3$ Exchange Interactions

Many proposals for inducing the Kitaev QSL state rely on manipulating the bond angles in Kitaev candidate materials to be closer to 90°. In order to assess whether this would be enough to induce a Kitaev QSL state, we used CSSD to examine the magnetic interactions of idealized versions of Na_2IrO_3 and α-$RuCl_3$.

To create these structures, we made versions of Na_2IrO_3 and α-$RuCl_3$ with Ir-O-Ir and Ru-Cl-Ru angles of 90°, with Ir-Ir and Ru-Ru bond lengths equal to the averages of those respective bond lengths in the relaxed structures, and with other parameters (such as interlayer distance) held constant.

We then performed CSSD on these two structures, using a similar process to the one we used with the relaxed structures. The one difference was in the initial step – only electronic structure was allowed to relax as ions were held constant.

Idealized Na_2IrO_3

In our initial comparison of various electronic relaxations of idealized Na_2IrO_3, there was a virtual tie for lowest energy (~0.1 meV difference per Ir) between one relaxation in which the spins pointed approximately along the a-axis of the unit cell, and one in which they pointed approximately along the b-axis of the unit cell. We therefore performed CSSD on both of these magnetic structures, and we report their results below. We also attempted to combine these data into one dataset for CSSD, but the relative error for the combined set was quite high (>40%), and therefore we are not reporting the combined results.

For the data with spins pointed near the a-axis (4.5% relative error):

Nearest neighbors (in meV/μ_B^2):

$$\mathbf{J_x} = \begin{bmatrix} 39 & 8 & -3 \\ 9 & 29 & 13 \\ -2 & 15 & 30 \end{bmatrix}, \quad \mathbf{J_y} = \begin{bmatrix} 29 & 9 & -13 \\ 8 & 39 & 3 \\ -15 & 2 & 30 \end{bmatrix}, \quad \mathbf{J_z} = \begin{bmatrix} 35 & 1 & 0 \\ 3 & 35 & 3 \\ -3 & 0 & 42 \end{bmatrix}.$$

Second-nearest neighbors (in meV/μ_B^2):

$$\mathbf{J_{2,1}} = \begin{bmatrix} 30 & 36 & -6 \\ 33 & 29 & 3 \\ -4 & 0 & -3 \end{bmatrix}, \quad \mathbf{J_{2,2}} = \begin{bmatrix} 31 & 33 & -3 \\ 33 & 31 & 3 \\ -4 & -3 & -2 \end{bmatrix}, \quad \mathbf{J_{2,3}} = \begin{bmatrix} 31 & 34 & 0 \\ 34 & 33 & 0 \\ -5 & 2 & -1 \end{bmatrix}.$$

Third-nearest neighbors (in meV/μ_B^2):

$$\mathbf{J_{3,1}} = \begin{bmatrix} 8 & 11 & 0 \\ 9 & 12 & 1 \\ -2 & -2 & -1 \end{bmatrix}, \quad \mathbf{J_{3,2}} = \begin{bmatrix} 7 & 9 & 0 \\ 10 & 7 & 2 \\ -2 & 0 & 0 \end{bmatrix}.$$

The largest term here is still J_1 (with an average value of 31 meV/μ_B^2), though this is considerably smaller than the value with the relaxed Na_2IrO_3 (56 and 43 meV/μ_B^2). K here is 9 meV/μ_B^2, still considerably smaller than J_1, and many of the off-diagonal terms (which have increased from before) are larger than this. There are also unusual anisotropic effects in the second-nearest-neighbor and third-nearest-neighbor interactions. In both, the off-diagonal terms are surprisingly large within the upper left 2x2 of the matrix, while the last diagonal term is surprisingly small. These unusual effects all point to anisotropy in orbital overlaps, which is likely caused by the strain put on the system from being forced to be idealized.

CSSD performed on the data with the spins pointed near the b-axis also shows unusual anisotropy (15% relative error):

Nearest neighbors (in meV/μ_B^2):

$$\mathbf{J_x} = \begin{bmatrix} 58 & 13 & 10 \\ 12 & 68 & -8 \\ 7 & -2 & 27 \end{bmatrix}, \quad \mathbf{J_y} = \begin{bmatrix} 68 & 12 & 8 \\ 13 & 58 & -10 \\ 2 & -7 & 27 \end{bmatrix}, \quad \mathbf{J_z} = \begin{bmatrix} 61 & 11 & -7 \\ 11 & 61 & 7 \\ -7 & 7 & 16 \end{bmatrix}.$$

Second-nearest neighbors (in meV/μ_B^2):

$$\mathbf{J_{2,1}} = \begin{bmatrix} 33 & 0 & -9 \\ 2 & 34 & 3 \\ -4 & 10 & 60 \end{bmatrix}, \quad \mathbf{J_{2,2}} = \begin{bmatrix} 31 & 6 & -8 \\ 0 & 32 & 6 \\ -6 & 6 & 53 \end{bmatrix}, \quad \mathbf{J_{2,3}} = \begin{bmatrix} 34 & 4 & -4 \\ 1 & 33 & 7 \\ -7 & 7 & 54 \end{bmatrix}.$$

Third-nearest neighbors (in meV/μ_B^2):

$$\mathbf{J_{3,1}} = \begin{bmatrix} 32 & 3 & 1 \\ 2 & 32 & 1 \\ 1 & -1 & 4 \end{bmatrix}, \quad \mathbf{J_{3,2}} = \begin{bmatrix} 31 & 9 & 0 \\ 7 & 31 & -2 \\ 2 & 0 & 7 \end{bmatrix}.$$

The third diagonal term is unusual here in every matrix – for the nearest neighbors and third-nearest neighbors, this terms is considerably smaller than would be expected, and for the second-nearest neighbors, it is considerably larger. While this anisotropy does make determining K somewhat harder, it can still be estimated by examining the difference between J_1 and $J_1 + K$ terms separately for the upper left 2x2 matrix, and the last diagonal term. Both of these methods indicate a K of approximately 11 meV/μ_B^2, which is similar to the value received from the calculation with the spins along the a-axis. This is considerably smaller than J_1, which has an average value of about 52 meV/μ_B^2 (though with large variance due to the above-mentioned anisotropy).

Idealized α-$RuCl_3$

CSSD with idealized α-$RuCl_3$ produced the following Hamiltonians with 12% relative error:

Nearest neighbors (in meV/μ_B^2):

$$\mathbf{J_x} = \begin{bmatrix} 50 & 9 & 13 \\ 9 & 50 & -15 \\ 13 & -15 & 32 \end{bmatrix}, \quad \mathbf{J_y} = \begin{bmatrix} 50 & 9 & 15 \\ 9 & 50 & -13 \\ 15 & -13 & 32 \end{bmatrix}, \quad \mathbf{J_z} = \begin{bmatrix} 50 & 7 & 3 \\ 7 & 50 & -13 \\ 13 & -13 & 25 \end{bmatrix}.$$

Second-nearest neighbors (in meV/μ_B^2):

$$\mathbf{J_{2,1}} = \begin{bmatrix} 30 & -2 & -5 \\ -2 & 30 & 5 \\ -5 & 5 & 39 \end{bmatrix}, \quad \mathbf{J_{2,2}} = \begin{bmatrix} 34 & -5 & -9 \\ -7 & 34 & 12 \\ -9 & 9 & 44 \end{bmatrix}.$$

Third-nearest neighbors (in meV/μ_B^2):

$$\mathbf{J_{3,1}} = \begin{bmatrix} 25 & 5 & 8 \\ 5 & 26 & -7 \\ 8 & -7 & 14 \end{bmatrix}, \quad \mathbf{J_{3,2}} = \begin{bmatrix} 25 & 4 & 6 \\ 4 & 25 & -6 \\ 6 & -6 & 17 \end{bmatrix}.$$

Compared to the relaxed α-$RuCl_3$ structure, the idealized α-$RuCl_3$ generally has similar interactions, but with a few notable differences. First, the off-diagonal terms are significantly larger in the idealized structure, though they are still smaller than the Heisenberg terms. Second, in the idealized structure, there is more anisotropy among the Heisenberg terms – the z-z terms (for nearest, second-nearest, and third-nearest interactions) are quite different than the other terms (~40% smaller for nearest- and third-nearest neighbors, and ~30% larger for second-nearest neighbors). Note that this is not the same as a Kitaev term – a nearest-neighbor Kitaev term would place the "odd-term-out" on a different interaction for the different interaction matrices, but here, the z-z interaction is always the odd-term-out. Both larger off-diagonal terms and more anisotropy among the Heisenberg terms are indicators of high anisotropy – which can probably be explained by the strained nature of this idealized structure. Of note, *K* is still small enough to be negligible.

	J_1	K	J_2	J_3	Unusual anisotropy?
Na_2IrO_3 (FM)	56	-18	26	1	N
Na_2IrO_3 (FM+AF)	43	3	28	1	N
Idealized Na_2IrO_3 (~a-axis)	31	9	20	5	Y
Idealized Na_2IrO_3 (~b-axis)	52	11	40	21	Y
α-$RuCl_3$	51	-6	30	30	N
Idealized α-$RuCl_3$	50	-4	45	21	Y

Table 1: Interaction terms found from CSSD. All reported values are in meV/μ_B^2.

Neither Na_2IrO_3 nor α-$RuCl_3$ appear to have significant Kitaev character, and neither do idealized versions of these structures. As the idealized version of these materials should see the isotropic portions of Ir-O-Ir interactions disappear, the dominant Heisenberg interactions presumably come from direct *d*-*d* hopping. While these 4*d* and 5*d* honeycomb materials are highly frustrated due to competing AF Heisenberg interactions, they appear unlikely enable a Kitaev QSL.

Possible Lanthanide Candidate Materials

4*f* honeycomb materials may have advantages over *d* honeycomb materials when it comes to fulfilling a Kitaev QSL state. First, the SOC is larger in *f*-orbitals. Second, *f*-orbitals are much more tightly bound, implying that the direct *f*-*f* orbital overlap (which contributes to Heisenberg-type interactions) would be significantly smaller than *d*-*d* overlap. We therefore investigated honeycomb lanthanides as potential Kitaev candidates (actinides were neglected due to their radioactivity).

We started our search by using Materials Project to identify lanthanide materials in a layered, honeycomb structure, and we found the following materials (with the following corresponding bond angles): Rb_2CeO_3 (~106°), $GdBr_3$ (~96°), Na_2TbO_3 (~98°), K_2TbO_3 (~105°), $YbBr_3$ (~97°), and $YbCl_3$ (~100° and ~113°).[36] For reference, Materials Project reports α-$RuCl_3$ and Na_2IrO_3 have bond angles of ~95° and ~101°, respectively.[36] Rb_2CeO_3 would be left with no valence electrons on the Ce^{4+}, so this material was dismissed. Of the remaining five materials, we chose to study $GdBr_3$, Na_2TbO_3, and $YbBr_3$, as these had bond angles significantly closer to 90° than the other two.

Under SOC, the seven *f*-orbitals split into three lower energy $j = 5/2$ states and four higher energy $j = 7/2$ states. Octahedral crystal field further splits the $j = 5/2$ states into two lower energy Γ_8 states and one higher energy Γ_7 state. The $j = 7/2$ states are split under the crystal field into one lower energy Γ_6 state, two middle energy Γ_8 states, and one higher energy Γ_7 state (Figure 18).[40]

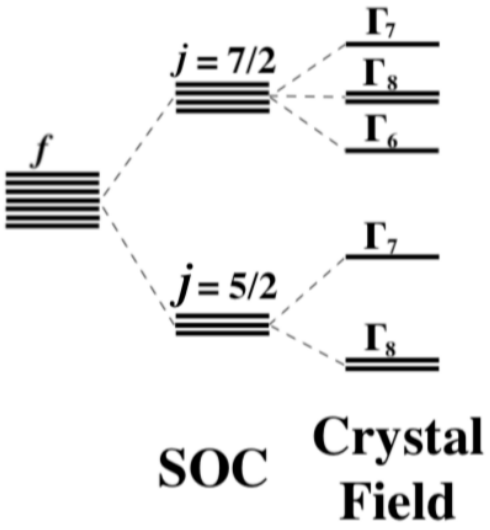

Figure 18: Proposed band structure for *f* orbitals under SOC and crystal field.

In $GdBr_3$, on the Gd^{3+}, the $4f^7$ electrons should fully fill the $j = 5/2$ states, and the Γ_6 state of $j = 7/2$ should be half filled, potentially allowing for Kitaev interactions. In Na_2TbO_3, the Tb^{4+} should also have $4f^7$ electrons, and thus may be expected to act similarly. In $YbBr_3$, on the Yb^{3+}, the $4f^{13}$ should fully fill the $j = 5/2$ states, along with the Γ_6 and Γ_8 states of $j = 7/2$. The highest state, Γ_7 of $j = 7/2$, should be half filled.

To investigate whether these descriptions of lanthanide honeycomb materials are accurate, we performed LSDA+*U*+SOC on VASP with these materials and a *k*-mesh of 4x2x4. We used a $U_{eff} = 6$ eV for our calculations, which is within the range used for

similar lanthanide materials within the literature. For $YbBr_3$, the unit cell contains three layers. To simplify our calculations, we used a reduced unit cell that contains only one layer, with the same interlayer distance.

Upon relaxation, we observed the multiple local-minima problem that we had previously seen with Na_2IrO_3, though, as expected, the problem was much more prevalent with these lanthanide materials. Additionally, relaxing these materials proved to be quite difficult, as the energies were prone to increase and the structures prone to "blow up" and "implode" upon attempts to relax the ions. In the end, we were unable to reliably relax $GdBr_3$ and Na_2TbO_3, but we had better success with $YbBr_3$. Of 12 initial $YbBr_3$ structures (magnetic moments initialized pointing in each of three directions and arranged in each of four magnetic structures), one "imploded" upon attempted relaxation, one "exploded," and the rest were all either fully relaxed or were mostly relaxed before the energy cycled between higher and lower values throughout attempted ionic relaxation (in which case we took the lowest energy ionic position as the relaxed one). Of the four tested magnetic structures (FM, Néel, stripy, zigzag), all were quite similar in energy, with stripy as the lowest energy, zigzag and Néel within the margin of error at 0.4 and 0.5 meV per Yb above the stripy phase in energy, and FM at 1.3 meV per Yb above stripy in energy. While these results must be approached with skepticism due to the small differences in energy and the difficulty in relaxing the structures, this does tentatively bode well for the possibility of achieving a Kitaev QSL state, as the stripy state is thought to be proximate to the Kitaev QSL state, and the zigzag and Néel states are thought to be closer than the FM state.

We calculated the band structure of this lowest-energy, stripy structure (Figure 19). While there was not as much separation between the j = 7/2 Γ_7 and Γ_8 states as may have been ideal, the band structure still generally follows the picture outlined above, with the j = 7/2 Γ_7 band split into what appear to be an upper Hubbard band and a lower Hubbard band.

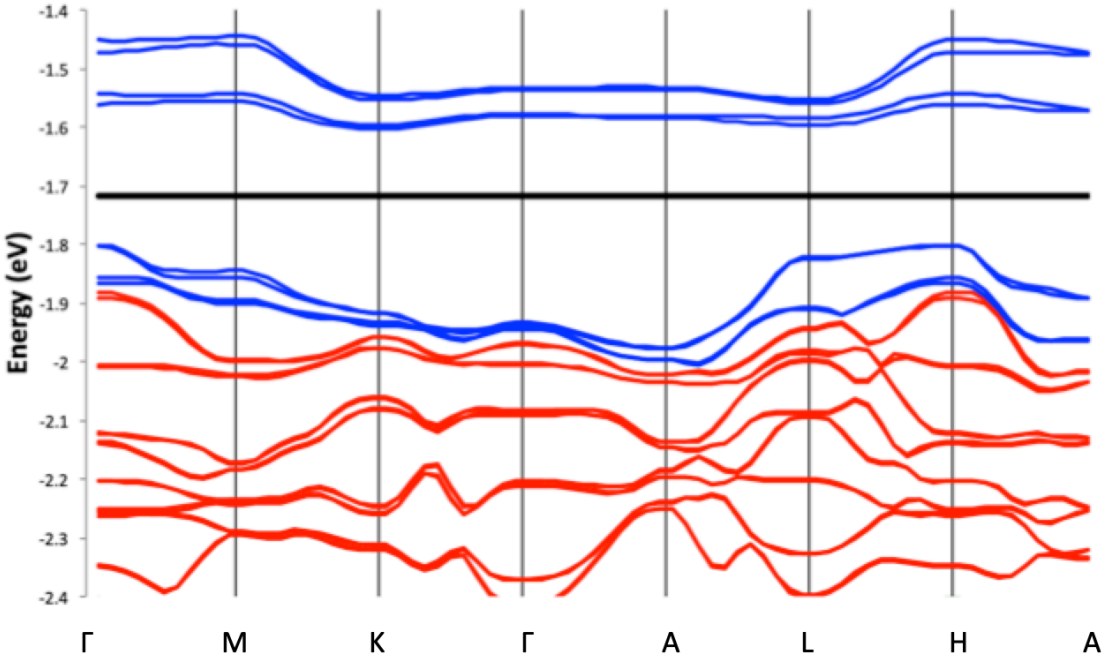

Figure 19: Calculated band structure of $YbBr_3$, showing the Γ_7 (blue) and Γ_8 (red) j = 7/2 bands. (k-paths determined with AFLOW.[33])

We additionally performed LSDA+SOC calculations on $YbBr_3$; without U, the band gap disappeared, indicating that $YbBr_3$ is indeed a Mott insulator. Unfortunately, this meant that we could not perform CSSD on $YbBr_3$, because our code for fixing magnetic moments in desired directions only works with U turned off, and doing so with $YbBr_3$ qualitatively changes the electronic character. Further research is necessary to determine if $YbBr_3$ or other lanthanide honeycomb materials can enable the Kitaev QSL state.

Conclusion

4*d* and 5*d* Kitaev candidate materials appear unlikely to allow for the Kitaev QSL phase. CSSD indicates these materials have small Kitaev interactions and large Heisenberg interactions. Proposed methods of manipulating these materials – such as by growing epitaxial layers on a substrate or applying strain – have problems. For epitaxial layers, Na_2IrO_3 cannot be cleanly separated into individual layers without significantly changing the band structure (in our calculations, from insulating to conducting). Regarding strain, in-plane compression increases the Heisenberg interaction from direct *d*-*d* orbital overlap, while tension increases the Ir-O-Ir angle further away from 90°. Even idealized versions of Na_2IrO_3 and α-$RuCl_3$ show very small Kitaev interactions and large Heisenberg interactions (as demonstrated via CSSD). *f*-orbital Kitaev candidate materials are worth investigating. It's possible that such materials have interactions that are simply too weak, creating an indifference to magnetic order, but such materials in all likelihood avoid one of the largest problems with *d*-materials – direct *f*-*f* orbital overlap is presumably very small, implying much smaller Heisenberg interaction competing with the Kitaev interaction.

References

[1] Chaloupka, J. *et al*, Kitaev-Heisenberg model on a honeycomb lattice: possible exotic phases in iridium oxides A_2IrO_3, *PRL*, **105**, 027204 (2010)

[2] Kitaev, A., Anyons in an exactly solved model and beyond, *Annals of Physics*, **321**, 2 (2006)

[3] Liu, X. *et al*, Long-range magnetic ordering in Na_2IrO_3, *Physical Review B*, **83**, 220403(R) (2011)

[4] Ye, F., *et al*., Direct evidence of a zigzag spin-chain structure in the honeycomb lattice: a neutron and x-ray diffraction investigation of singe-crystal Na_2IrO_3, *Physical Review B*, **85**, 180403(R) (2012)

[5] Yamaji, Y. *et al*., Clues and criteria for designing a Kitaev spin liquid revealed by thermal and spin excitations of the honeycomb iridate Na_2IrO_3, *Physical Review B*, **93**, 174425 (2016)

[6] Kasahara, Y. *et al*., Majorana quantization and half-integer thermal quantum Hall effect in a Kitaev spin liquid, *Nature*, **559**, 227 (2018)

[7] Shor, P. W., Algorithms for Quantum Computation: Discrete Logarithms and Factoring, *Proceedings 35th Annual Symposium on Foundations of Computer Science*, Santa Fe, NM, USA, 124 (1994)

[8] Kassal, I. *et al*., Polynomial-time quantum algorithm for the simulation of chemical dynamics, *PNAS*, **105** (48), 18681 (2008)

[9] Arute, F. *et al*., Quantum supremacy using a programmable superconducting processor, *Nature*, **574**, 505 (2019)

[10] Momma, K. and Izumi, F., VESTA 3 for three-dimensional visualization of crystal, volumetric and morphology data, *Journal of Applied Crystallography*, **44**, 1272 (2011)

[11] Shitade, A. *et al*., Quantum spin hall effect in a transition metal oxide Na_2IrO_3, *PRL*, **102**, 256403 (2009)

[12] Jackeli, G. and Khaliullin, G., Mott Insulators in the Strong Spin-Orbit Coupling Limit: From Heisenberg to a Quantum Compass and Kitaev Models, *PRL*, **102**, 017205 (2009)

[13] Chaloupka, J. *et al*., Zigzag magnetic order in the iridium oxide Na_2IrO_3, *PRL*, **110**, 097204 (2013)

[14] Kimchi, I. and You, Y.-Z., Kitaev-Heisenberg-J_2-J_3 model for the iridates A_2IrO_3, *Physical Review B*, **84**, 180407(R) (2011)

[15] Comin, R. *et al*., Na_2IrO_3 as a novel relativistic Mott insulator with a 340-meV gap, *PRL*, **109**, 266406 (2012)

[16] Kim, M. *et al*., Insulating nature of Na_2IrO_3: Mott-type or Slater-type, *Physical Review B*, **93**, 195135 (2016)

[17] Kim, H.-J. *et al*., Antiferromagnetic Slater insulator phase of Na_2IrO_3, *Scientific Reports*, **4**, 5253 (2014)

[18] Mazin, I. I. *et al*., Origin of the insulating state in honeycomb iridates and rhodates, *Physical Review B*, **88**, 035115 (2013)

[19] Kim, H.-S. and Kee, H.-Y., Crystal structure and magnetism in α-$RuCl_3$: An *ab initio* study, *Physical Review B*, **93**, 155143 (2016)

[20] Kresse, G. and Hafner, J., Ab initio molecular dynamics for liquid metals, *Physical Review B*, **47**, 558 (1993)

[21] Kresse, G. and Hafner, J., Ab initio molecular-dynamics simulation of the liquid-metal-amorphous-semiconductor transition in germanium, *Physical Review B*, **49**, 14251 (1994)

[22] Kresse, G. and Furthmüller, J., Efficiency of ab-initio total energy calculations for metals and semiconductors using a plane-wave basis set, *Computational Materials Science*, **6**, 15 (1996)

[23] Kresse, G. and Furthmüller, J., Efficient iterative schemes for ab initio total-energy calculations using a plane-wave basis set, *Physical Review B*, **54**, 11169 (1996)

[24] Perdew, J. P. and Zunger, A., Self-interaction correction to density-functional approximations for many-electron systems, *Physical Review B*, **23,** 5048 (1981)

[25] Hohenberg, P. and Kohn, W. Inhomogeneous electron gas, *Physical Review*, **136** (3B), 864, (1964)

[26] Kohn, W. and Sham, L. J. Self-consistent equations including exchange and correlation effects, *Physical Review*, **140** (4A), 1133, (1965)

[27] Dudarev, S. L. *et al*., Electron-energy-loss spectra and the structural stability of nickel oxide: an LSDA+*U* study, *Physical Review B*, **57** (3), 1505 (1998)

[28] Blöchl, P. E., Projector augmented-wave method, *Physical Review B*, **50**, 17953 (1994)

[29] Mazin, I. I. *et al*., Na_2IrO_3 as a molecular orbital crystal, *PRL*, **109**, 197201 (2012)

[30] Hu, K. *et al*., First-principles study of the magnetic structure of Na_2IrO_3, *PRL*, **115**, 167204 (2015)

[31] Foyevtsova, K. *et al*., *Ab initio* analysis of the tight-binding parameters and magnetic interactions in Na_2IrO_3, *Physical Review B*, **88**, 035107 (2013)

[32] Fei, Z. and Ozolins, V., Crystal field and magnetic structure of UO_2, *Physical Review B*, **83**, 085106 (2011)

[33] Curarolo, S. *et al*., AFLOW: an automatic framework for high-throughput materials discovery, *Computational Materials Science*, **58**, 218 (2012)

[34] Fouet, J. B. *et al*., An investigation of the quantum J_1-J_2-J_3 model on a honeycomb lattice, *The European Physical Journal B*, **20**, 241 (2001)

[35] Reuther, J. *et al*., Spiral order in the honeycomb iridate Li_2IrO_3, *Physical Review B*, **90**, 100405(R) (2014)

[36] Jain, A. *et al*., The Materials Project: A materials genome approach to accelerating materials innovation, *APL Materials*, **1**, 011002 (2013)

[37] Yadav, R. *et al*., Strain- and pressure-tuned magnetic interactions in honeycomb Kitaev materials, *Physical Review B*, **98**, 121107(R) (2018)

[38] Singh, Y., *et al*., Relevance of the Heisenberg-Kitaev Model for the Honeycomb Lattice Iridates A_2IrO_3, *PRL*, **108**, 127203 (2012)

[39] Woo, S., *et al*., Poisson's ratio in layered two-dimensional crystals, *Physical Review B*, **93**, 075420 (2016)

[40] Tanaka, K. and Takenaka, Y. (2012). XAO Analysis – AO's and Their Populations in Crystal Fields. In Benedict, J. B. (Ed.), *Recent Advances in Crystallography* (pp. 282). Rijeka, Croatia: InTech.